



AFRL-AFOSR-VA-TR-2021-0096

---

## A Unified, Universal Model for Electron Emission and Breakdown

**Garner, Allen**  
**PURDUE UNIVERSITY**  
**155 S GRANT ST**  
**WEST LAFAYETTE, IN, 47907**  
**USA**

---

**08/07/2021**  
**Final Technical Report**

DISTRIBUTION A: Distribution approved for public release.

Air Force Research Laboratory  
Air Force Office of Scientific Research  
Arlington, Virginia 22203  
Air Force Materiel Command

**REPORT DOCUMENTATION PAGE**Form Approved  
OMB No. 0704-0188

The public reporting burden for this collection of information is estimated to average 1 hour per response, including the time for reviewing instructions, searching existing data sources, gathering and maintaining the data needed, and completing and reviewing the collection of information. Send comments regarding this burden estimate or any other aspect of this collection of information, including suggestions for reducing the burden, to Department of Defense, Washington Headquarters Services, Directorate for Information Operations and Reports (0704-0188), 1215 Jefferson Davis Highway, Suite 1204, Arlington, VA 22202-4302. Respondents should be aware that notwithstanding any other provision of law, no person shall be subject to any penalty for failing to comply with a collection of information if it does not display a currently valid OMB control number.

**PLEASE DO NOT RETURN YOUR FORM TO THE ABOVE ADDRESS.**

1. REPORT DATE (DD-MM-YYYY) 07-08-2021	2. REPORT TYPE Final	3. DATES COVERED (From - To) 01 Mar 2018 - 31 Aug 2021
4. TITLE AND SUBTITLE A Unified, Universal Model for Electron Emission and Breakdown		5a. CONTRACT NUMBER
		5b. GRANT NUMBER FA9550-18-1-0218
		5c. PROGRAM ELEMENT NUMBER 61102F
6. AUTHOR(S) Allen Garner		5d. PROJECT NUMBER
		5e. TASK NUMBER
		5f. WORK UNIT NUMBER
7. PERFORMING ORGANIZATION NAME(S) AND ADDRESS(ES) PURDUE UNIVERSITY 155 S GRANT ST WEST LAFAYETTE, IN 47907 USA		8. PERFORMING ORGANIZATION REPORT NUMBER
9. SPONSORING/MONITORING AGENCY NAME(S) AND ADDRESS(ES) AF Office of Scientific Research 875 N. Randolph St. Room 3112 Arlington, VA 22203		10. SPONSOR/MONITOR'S ACRONYM(S) AFRL/AFOSR RTB1
		11. SPONSOR/MONITOR'S REPORT NUMBER(S) AFRL-AFOSR-VA-TR-2021-0096

**12. DISTRIBUTION/AVAILABILITY STATEMENT**

A Distribution Unlimited: PB Public Release

**13. SUPPLEMENTARY NOTES****14. ABSTRACT**

This effort has focused on assessing the impact of submicroscale phenomena on gas breakdown and electron emission, specifically the transition between mechanisms in the presence of collisions, which are important for microplasma devices as the effective gap decreases below one micron where space charge may dominate over field emission and for vacuum electronics devices where leakage may result in collisions.

Year 1 focused on incorporating collisions into analytic equations describing the transition from the Fowler-Nordheim (FN) equation to the Child-Langmuir (CL) law for vacuum space-charge limited emission (SCLE) at high mobility  $\frac{1}{4}$ , and the Mott-Gurney (MG) law for collisional SCLE at low  $\frac{1}{4}$ . We also observed a nexus where the asymptotic solutions of all three electron emission regimes converge with a unique value of  $V$ ,  $\frac{1}{4}$  or gap distance  $D$ . We next extended this to include resistance to account for the series resistors used to mitigate the rapid increase in current density that reduces device stability, demonstrating the transition to Ohm's law for high resistance.

In Year 2, we extended the emission theory from Year 1 by incorporating (1) thermionic emission and (2) quantum effects in SCLE by Schrodinger's equation, (3) applying the theory to liquids, and (4) beginning our analysis of SCLE for non-planar geometries using variational calculus. By using the generalized thermo-field (GTF) model for electron emission, we demonstrated the transitions between Richard-Lau-Dushman (RLD), FN, CL, MG, and OL asymptotically and published this work in Physical Review Research during Year 3. We also incorporated quantum effects into our nexus theory, which is currently under review. To assess the broad applicability of this theory, we have also applied the general emission theory to liquids, which also undergo field emission and MG.

This work was published in the Journal of Applied Physics during Year 3. In Year 3, we completed and published the efforts on unifying thermionic emission with nexus theory, apply nexus theory to liquids and systems undergoing phase changes from liquids to gases, and applying conformal mapping to non-planar geometries. Additionally, we published a tutorial on microscale gas breakdown in IEEE Transactions on Plasma Science, an invited Perspective in the Journal of Applied Physics unifying breakdown theory to emission nexus theory, and an invited Perspective in the Journal of Applied Physics (selected as Editor's Pick) on space-charge limited emission. Also in Year 3, we extended the microscale gas breakdown theory from Year 1 to a pin-to-plate geometry, using the work function as the fitting parameter rather than field enhancement; the manuscript was accepted in a special issue on low-temperature plasma physics in the Journal of Applied Physics. We are currently working to incorporate an external series resistor into the planar theory and particle-in-cell simulations. New work ongoing in Year 3 has involved applying variational calculus and conformal mapping to derive equations for space-charge limited current for finite 2D and 3D emitters and are preparing a manuscript to submit to Physical Review Applied. We also are drafting a manuscript for Applied Physics Letters based on work applying variational calculus and conformal mapping to derive equations for pin-to-plate, pin-to-pin, and misaligned geometries. This work has direct application to directed energy systems and we are actually leveraging this result on another effort for developing a computational model for an atmospheric pressure plasma with a pin-to-plate system. Finally, we incorporated photoemission into the aforementioned nexus theory and working to develop all the various nexuses to prepare a manuscript for submission.

For the final period of performance during the no-cost extension, we have worked on finalizing multiple manuscripts with some likely to be submitted for publication after the period of performance. These include efforts on incorporating a series resistor into microscale gas breakdown theory and using one-dimensional (1-D) particle-in-cell simulations to determine

During this grant, we have published ten refereed journal articles; have five more submitted or in preparation; and presented (or will present) 1 conference plenary talk, 3 invited conference talks, 13 invited seminars, 1 conference minicourse, 23 contributed conference oral presentations, and 7 conference posters. We have partially funded five graduate students and four undergraduate students (co-funded by AFOSR and the Purdue Summer Undergraduate Research Fellowship) throughout this period and worked with another undergraduate student through research for credit. One graduate student funded under this grant has received the Purdue University Doctoral Fellowship and American Nuclear Society Graduate Scholarship and a second received three Directed Energy Professional Society Scholarships and the 2020 College of Engineering Graduate Research Award. One PhD student and one M.S. student funded by this grant have graduated. During this time, Dr. Garner was promoted to Associate Professor with tenure and received the 2019 Outstanding Faculty Mentor of Engineering Graduate Students (Purdue University Engineering Graduate Programs) and the 2021 Purdue School of Nuclear Engineering Outstanding Research Award.

**15. SUBJECT TERMS**

16. SECURITY CLASSIFICATION OF:			17. LIMITATION OF ABSTRACT	18. NUMBER OF PAGES	19a. NAME OF RESPONSIBLE PERSON
a. REPORT	b. ABSTRACT	c. THIS PAGE			ALI SAYIR
U	U	U	UU	43	19b. TELEPHONE NUMBER (Include area code) 426-7236

Standard Form 298 (Rev.8/98)

Prescribed by ANSI Std. Z39.18

# A Unified, Universal Model for Electron Emission and Breakdown

## ANNUAL REPORT

FA9550-18-1-0218

Period of Performance: March 1, 2018 to August 31, 2021

Prepared by:

Dr. Allen L. Garner, Principal Investigator  
Associate Professor and Undergraduate Program Chair, School of Nuclear Engineering  
Purdue University  
516 Northwestern Ave.  
West Lafayette, IN 47906  
Tel: (765) 494-0618  
Email: algarner@purdue.edu



This material is based upon work supported by the Air Force Office of Scientific Research under award number FA9550-18-1-0218. The views and conclusions contained herein are those of the authors only and should not be interpreted as representing those of AFOSR, the U.S. Air Force, or the U.S. Government.

## ABSTRACT

This effort has focused on assessing the impact of submicroscale phenomena on gas breakdown and electron emission, specifically the transition between mechanisms in the presence of collisions, which are important for microplasma devices as the effective gap decreases below one micron where space charge may dominate over field emission and for vacuum electronics devices where leakage may result in collisions.

Year 1 focused on incorporating collisions into analytic equations describing the transition from the Fowler-Nordheim (FN) equation to the Child-Langmuir (CL) law for vacuum space-charge limited emission (SCLE) at high mobility  $\mu$ , and the Mott-Gurney (MG) law for collisional SCLE at low  $\mu$ . We also observed a nexus where the asymptotic solutions of all three electron emission regimes converge with a unique value of  $V$ ,  $\mu$  or gap distance  $D$ . We next extended this to include resistance to account for the series resistors used to mitigate the rapid increase in current density that reduces device stability, demonstrating the transition to Ohm's law for high resistance.

In Year 2, we extended the emission theory from Year 1 by incorporating (1) thermionic emission and (2) quantum effects in SCLE by Schrodinger's equation, (3) applying the theory to liquids, and (4) beginning our analysis of SCLE for non-planar geometries using variational calculus. By using the generalized thermo-field (GTF) model for electron emission, we demonstrated the transitions between Richard-Lau-Dushman (RLD), FN, CL, MG, and OL asymptotically and published this work in *Physical Review Research* during Year 3. We also incorporated quantum effects into our nexus theory, which is currently under review. To assess the broad applicability of this theory, we have also applied the general emission theory to liquids, which also undergo field emission and MG. This work was published in the *Journal of Applied Physics* during Year 3.

In Year 3, we completed and published the efforts on unifying thermionic emission with nexus theory, apply nexus theory to liquids and systems undergoing phase changes from liquids to gases, and applying conformal mapping to non-planar geometries. Additionally, we published a tutorial on microscale gas breakdown in *IEEE Transactions on Plasma Science*, an invited Perspective in the *Journal of Applied Physics* unifying breakdown theory to emission nexus theory, and an invited Perspective in the *Journal of Applied Physics* (selected as Editor's Pick) on space-charge limited emission. Also in Year 3, we extended the microscale gas breakdown theory from Year 1 to a pin-to-plate geometry, using the work function as the fitting parameter rather than field enhancement; the manuscript was accepted in a special issue on low-temperature plasma physics in the *Journal of Applied Physics*. We are currently working to incorporate an external series resistor into the planar theory and particle-in-cell simulations. New work ongoing in Year 3 has involved applying variational calculus and conformal mapping to derive equations for space-charge limited current for finite 2D and 3D emitters and are preparing a manuscript to submit to *Physical Review Applied*. We also are drafting a manuscript for *Applied Physics Letters* based on work applying variational calculus and conformal mapping to derive equations for pin-to-plate, pin-to-pin, and misaligned geometries. This work has direct application to directed energy systems and we are actually leveraging this result on another effort for developing a computational model for an atmospheric pressure plasma with a pin-to-plate system. Finally, we incorporated photoemission into the

aforementioned nexus theory and working to develop all the various nexuses to prepare a manuscript for submission.

For the final period of performance during the no-cost extension, we have worked on finalizing multiple manuscripts with some likely to be submitted for publication after the period of performance. These include efforts on incorporating a series resistor into microscale gas breakdown theory and using one-dimensional (1-D) particle-in-cell simulations to determine

During this grant, we have published ten refereed journal articles; have five more submitted or in preparation; and presented (or will present) 1 conference plenary talk, 3 invited conference talks, 13 invited seminars, 1 conference minicourse, 23 contributed conference oral presentations, and 7 conference posters. We have partially funded five graduate students and four undergraduate students (co-funded by AFOSR and the Purdue Summer Undergraduate Research Fellowship) throughout this period and worked with another undergraduate student through research for credit. One graduate student funded under this grant has received the Purdue University Doctoral Fellowship and American Nuclear Society Graduate Scholarship and a second received three Directed Energy Professional Society Scholarships and the 2020 College of Engineering Graduate Research Award. One PhD student and one M.S. student funded by this grant have graduated. During this time, Dr. Garner was promoted to Associate Professor with tenure and received the 2019 Outstanding Faculty Mentor of Engineering Graduate Students (Purdue University Engineering Graduate Programs) and the 2021 Purdue School of Nuclear Engineering Outstanding Research Award.

## INTRODUCTION

The continuing diversification in size, pressure, and power requirements of electronic devices motivates the unification of various breakdown and electron emission models to optimize device design and operation [1]. Classical theory predicts electric discharges based upon Townsend avalanche (TA), represented mathematically by Paschen's law (PL) [2]. At microscale, field emission (FE), the stripping of electrons from the cathode modeled by the Fowler-Nordheim (FN) equation, drives breakdown [1,3-12].

This grant first assessed the transition between electron emission mechanisms rather than providing exact predictions, which would require the application of more recent advances in FN theory [13-15]. We first elucidated the effect of pressure on these transitions between mechanisms. At vacuum, studies demonstrated that increasing current makes electron emission limited by space charge [16], as described by the Child-Langmuir (CL) law [17,18]. Electron emission is critical in vacuum electronics [19-22], with many studies exploring the importance of space charge on thermionic emission (TE) [23-28] and examining the transition from FE to space-charge limited emission (SCLE) [29-34] and FE to TE [35]. An asymptotic analysis derived an equation for the transition from FE to SCLE for increasing voltage  $V$  or decreasing  $D$  [17]. Moreover, as one reduces gap distances below microscale, gas breakdown will transition from FE [3,5,6,36] to SCLE, particularly for  $D \sim \lambda$ , which is the mean-free path. However, for  $D > \lambda$ , SCLE must account for collisions [37-38]. While several studies have corrected the CL law for collisions [39-41], a better analogy is SCLE in semiconductors, given by the Mott-Gurney (MG) law [42]. A matched asymptotic analysis of plasma sheath behavior showed that the maximum current density  $J$  transitions from CL scaling,  $J \propto V^{3/2}/D^2$ , to MG scaling,  $J \propto V^2/D^3$ , by incorporating electron

mobility  $\mu$ , defined as  $v_d = \mu E$  where  $v_d$  is drift velocity and  $E$  is electric field, into the fluid equation for electron motion [43].

In practical devices, electron emission current density increases rapidly with voltage, necessitating the addition of a series resistor to improve stability [44]; however, this may increase operating voltage and cost while reducing efficiency [45]. Similarly, one may add an external resistor to control device current in microplasma devices [46-47]. Experiments using an external resistor to generate a microplasma [46] motivated one-dimensional planar particle-in-cell (PIC) simulations incorporating an external resistor [47] with good agreement with experimental results [46]; however, the conditions were not in the field emission dominated regime.

Thus, previous asymptotic studies demonstrated the transition from FN to CL [17] and CL to MG [43]. We first comprehensively assessed the transition between all three electron emission mechanisms and incorporated a resistance in series to assess “nexuses” between the dominant mechanisms, which we published in Year 2 [48]. In Year 2, we completed and published the incorporation of resistance into this theory [49]. In Year 3, we completed and published the incorporation of thermionic emission into this theoretical construct [50] and began incorporating photoemission [51]. We also successfully applied conformal mapping to derive analytic solutions for space-charge limited current (SCLC) in vacuum for various non-planar geometries [52], including validating the equation for SCLC for concentric cylinders derived using variational calculus [53]. Finally, we extend our previous derivation of microscale gas breakdown for planar geometries [54] to pin-to-plate geometries [55] that are more experimentally relevant [56].

## NEXUS THEORY OVERVIEW

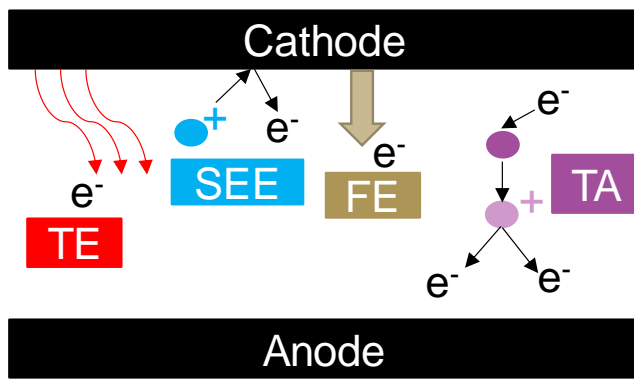


FIG. 1. Schematic of the mechanisms involved in microscale gas breakdown, including thermionic emission (TE), ion-induced secondary electron emission (SEE), field emission (FE), and collisions (TA) [57].

understanding the interplay between these mechanisms is important. This has motivated a detailed, comprehensive assessment of electron emission and gas breakdown mechanisms using the framework summarized in Fig. 1 [57].

A majority of the efforts on this grant have focused on connecting various emission and breakdown mechanisms. We have dubbed the assessment of these transitions as “nexus theory,” since they generally involve examining the intersection of the asymptotic solutions typically taken as representative for a given phenomenon, such as Child-Langmuir for vacuum SCLC, Mott-Gurney for collisional SCLC, as Fowler-Nordheim for field emission. Although gas breakdown is not an electron emission mechanism, electron emission does contribute to gas breakdown for microscale and smaller gaps, so

The drive toward smaller devices and incorporating more complete physics for developing predictive theories and simulations has motivated effort to develop a single framework for coupling the mechanisms outlined in Fig. 2. While Fig. 2 outlines general trends in mechanisms, it is important to realize that these transitions may not always occur in this manner, which further motivates increasingly complete models. As described above, when considering collisions, sufficiently high  $\mu$  or sufficiently low  $d$  may cause FE to directly transition to CL even at non-vacuum pressures [48]. As discussed above, thermionic emitters sometimes undergo transition from TE to FE; under other conditions, TE transitions directly to CL.

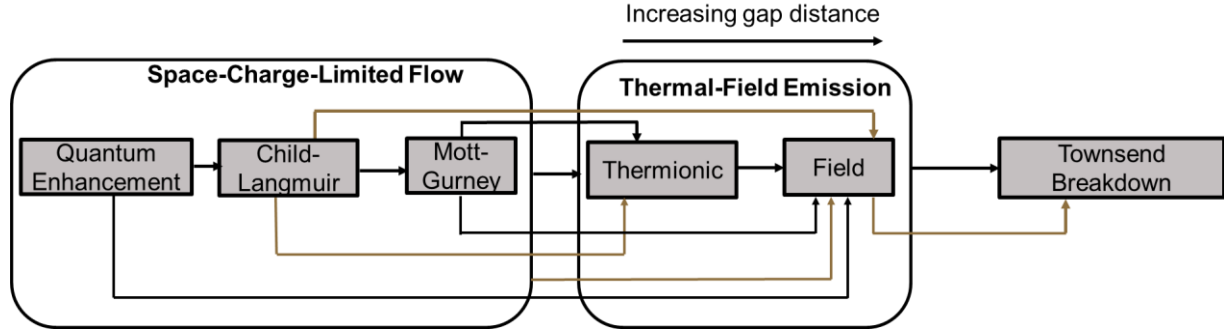


FIG. 2. Schematic demonstrating the typical transition in electron emission mechanisms from quantum-enhanced space-charge limited flow to Townsend avalanche as a function of temperature and gap distance. The exact mechanistic transitions may vary depending on the specific pressure, temperature, gap distance, and bias voltage in the gap. Figure adapted from Ref. [57].

Over the course of this effort, we have worked to achieve the linkages summarized in Fig. 2. The following sections highlight these efforts, which have been reported in more detail in the relevant previous annual reports.

### NEXUS THEORY: UNIFICATION OF FIELD EMISSION WITH SPACE-CHARGE LIMITED EMISSION WITH COLLISIONS

[A. M. Darr, A. M. Loveless, and A. L. Garner, “Unification of field emission and space charge limited emission with collisions,” Appl. Phys. Lett. **114**, 014103 (2019).]

We considered a one-dimensional, planar diode filled with a neutral gas with electron mobility  $\mu$ , which varies inversely with pressure  $P$  [48], and a cathode at  $x = 0$  and anode at  $x = D$ , fixed at  $V$  with respect to the cathode. We further assume electron emission from the cathode with negligible initial ( $t = 0$ ) velocity and accelerated by the surface electric field,  $E_s = E(0)$ , or  $x(0) = 0, v(0) = 0, a(0) = eE_s/m$ . We then combined Poisson’s equation with the force law for an electron exposed an electric field and collisions with neutral gas atoms, revising the conservation of energy approach used in vaccum [17] to give

$$m \frac{dv}{dt} = e \frac{d\phi}{dx} - \frac{ev}{\mu}, \quad (1)$$

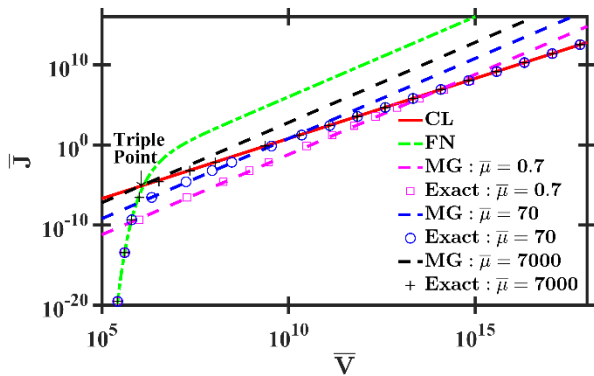


FIG. 3. Dimensionless current density  $\bar{J}$  as a function of dimensionless voltage  $\bar{V}$  for the exact solution of (9) and the asymptotic solutions of (7)-(9) for Child-Langmuir (CL), Fowler-Nordheim (FN), and Mott-Gurney (MG), respectively for three different dimensionless mobilities  $\bar{\mu}$  at  $\bar{D} = 10^7$ . For increasing  $\bar{V}$ , electron emission transitions from FN to MG to CL with electron emission always driven by FN and CL at sufficiently low and high voltages, respectively. A specific combination of  $\bar{\mu}$ ,  $\bar{D}$ , and  $\bar{V}$ ,  $\bar{J}_{FN} = \bar{J}_{MG} = \bar{J}_{CL}$  yields a “triple point” where all three asymptotic solutions match [from Ref. [48]].

emission transitions from FN to CL directly, just as at vacuum. Fig. 3 shows that this transition corresponds to MG = CL = MG, which we initially referred to as a “triple point,” but now refer to as a third-order nexus because three asymptotic solutions match.

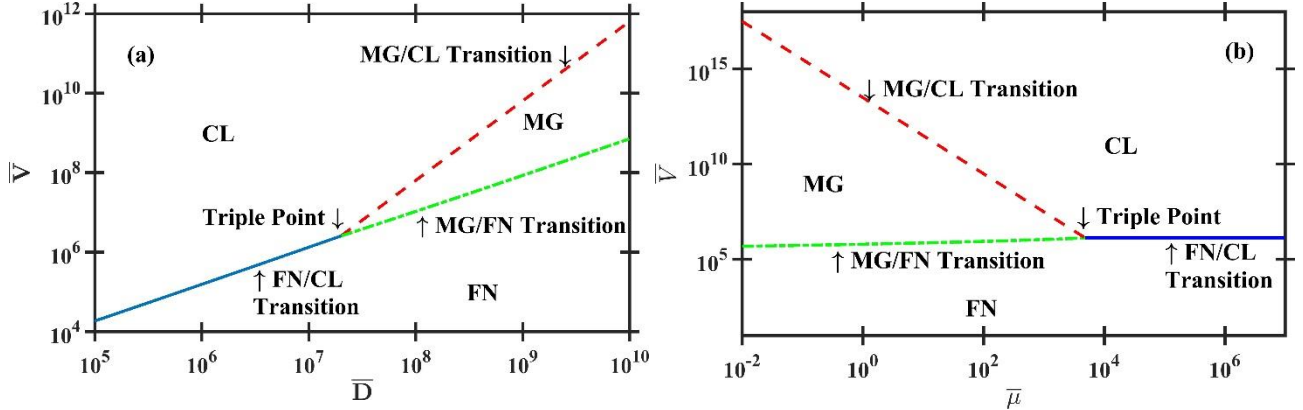


FIG. 4. Dimensionless voltage  $\bar{V}$  as a function of dimensionless gap distance  $\bar{D}$  for dimensionless mobility  $\bar{\mu} = 7 \times 10^3$  (a) or as a function of  $\bar{\mu}$  at  $\bar{D} = 10^7$  (b). At small  $\bar{D}$  or high  $\bar{\mu}$  (or low pressure,  $P$ , since  $P \propto 1/\bar{\mu}$ ), collisions are not important and electron emission directly transitions from Fowler-Nordheim (FN) to Child-Langmuir (CL), as in vacuum. At the triple point, Mott-Gurney (MG) becomes important due to collisions and FN = CL = MG. At larger gaps or lower  $\mu$  (higher  $P$ ), raising  $\bar{V}$  causes emission to transition from FN to MG to CL, indicating that one can achieve CL if the electron energy is sufficiently large to minimize collisions with the neutral gas [From Ref. [48]].

To determine the conditions for the transitions between these emission mechanisms, we matched the relevant asymptotic solutions. This also provides the conditions where the full theory had to

where  $\mu$  is electron mobility. We then nondimensionalized the relevant equations and obtained asymptotic solutions for Child-Langmuir (CL) in limits of high applied voltage, high mobility, and/or small gap distance, Mott-Gurney (MG) in limits of low mobility and high applied voltage/small gap distance, and Fowler-Nordheim (FN) for low voltage or large gap distance. Fig. 3 shows the transition for a plot of current density as a function of applied voltage for a given gap distance where the emission mechanism transitions from FN at low voltages to MG at higher voltages and lower mobilities to CL at higher voltage and/or higher mobility. For a given mobility, the FN to MG transition vanishes and

emission transitions from FN to CL directly, just as at vacuum. For higher mobilities, the gap

behaves as vacuum. Fig. 3 shows that this transition corresponds to MG = CL = MG, which we initially referred to as a “triple point,” but now refer to as a third-order nexus because three asymptotic solutions match.

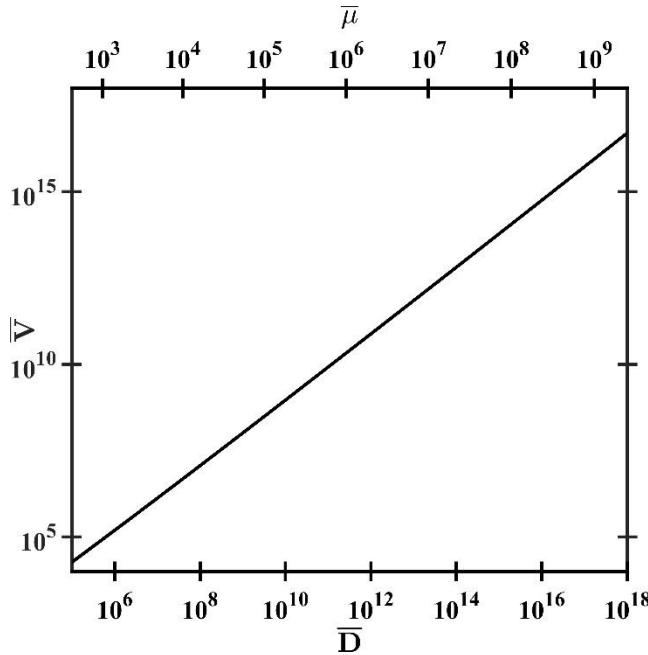


FIG. 5. Dimensionless voltage  $\bar{V}$  as a function of dimensionless gap distance  $\bar{D}$  and dimensionless mobility  $\bar{\mu}$  describing the triple point. The triple point, where electron emission is identically defined by Child-Langmuir (CL), Mott-Gurney (MG), and Fowler-Nordheim (FN), is fully specified by  $\bar{V}$ ,  $\bar{D}$ , or  $\bar{\mu}$  [From Ref. [48]].

These results indicate the triple point for a 250 nm diode filled with nitrogen occurs near atmospheric pressure. This is particularly relevant for microscale gas breakdown, where one generally transitions from Townsend avalanche to field emission for  $D$  on the order of microns [1,3-6]. As one continues reducing gap distance at atmospheric pressure, one would anticipate transitioning from FE to SCLE. At sufficiently low  $D$ , collisions become unimportant and SCLE transitions from MG to CL. The calculations above indicate that reducing  $D$  from approximately 1  $\mu\text{m}$  to 250 nm for nitrogen causes electron emission to transition from FE to the triple point, suggesting that further reducing gap size results in vacuum-like electron emission even at atmospheric pressure.

Even microscale gaps at atmospheric pressure can exhibit transitions between FN, MG, and CL. For an atmospheric pressure nitrogen-filled diode with  $D = 1 \mu\text{m}$  ( $\bar{D} = 6.90 \times 10^8$ ), solving for the transitions from FN to MG, MG to CL, and CL to FN, respectively, gives  $\bar{V} = 6.74 \times 10^7$  ( $V = 1.79 \text{ kV}$ ),  $\bar{V} = 3.10 \times 10^8$  ( $V = 8.24 \text{ kV}$ ), and  $\bar{V} = 7.25 \times 10^7$  ( $V = 1.93 \text{ kV}$ ) respectively. Since the gap distance is larger than that of the triple point, FN transitions to MG at a lower voltage than expected from CL [17]. This further demonstrates that even at high  $PD$ , emission behavior can still follow CL for sufficiently high voltage, even at larger gaps and higher pressures.

be solved analytically due to the contribution of multiple mechanisms; far away from these intersections, one may safely use the relevant asymptotic solution (CL, MG, or FN). Fig. 4 shows examples of these phase space plots for voltage as a function of gap distance and voltage as a function of mobility. The gap distance plot shows that gap distances below the “triple point” causes the gap to behave like vacuum with FN transitioning directly to CL. Similarly, the mobility plot shows that a mobility beyond that corresponding to the “triple point” makes the gap appear like vacuum, causing electron emission to transition directly from FN to CL. This third-order nexus is uniquely defined by the pressure, gap distance, or mobility; selecting any one of these parameters yields the other two. Fig. 5 shows the conditions for the third-order nexus.

## NEUXS THEORY: INCORPORATING A SERIES RESISTOR INTO THE THEORY FOR SPACE CHARGE LIMITED EMISSION TO FIELD EMISSION WITH COLLISIONS

[S. D. Dynako, A. M. Darr, and A. L. Garner, “Incorporating Resistance into the Transition from Field Emission to Space Charge Limited Emission with Collisions,” IEEE J. Electron Dev. Soc. **7**, 650-654 (2019).]

The immediately preceding section considered a one-dimensional, planar diode filled with a neutral gas with electron mobility  $\mu$ , which varies inversely with pressure  $P$  [48], and a cathode at  $x = 0$  and anode at  $x = D$ , fixed at  $V_g$  with respect to the cathode. We next consider the effect of a series resistor, which is often used to limit currents to field emitters to prevent damage. In this case, we consider the external resistor  $R$  to be in series with the diode with impedance  $Z$  that is a function of  $V_g$ ; therefore, the applied voltage  $V_{app} \neq V_g$  and is instead given by

$$V_{app} = V_g + IR = I(Z + R), \quad (2)$$

with  $Z \equiv V_g/(JS)$  and current  $I \equiv JS$  for emitter surface area  $S$  [49]. For nondimensional resistance  $\bar{R} = 0$ ,  $\bar{V}_g \equiv \bar{V}_{app}$ . When  $R \gg Z$ , the entire circuit will tend toward Ohm’s law (OL), or, in nondimensional units

$$\bar{J}_{Ohm} = \bar{V}_{app}/\bar{R}, \quad (3)$$

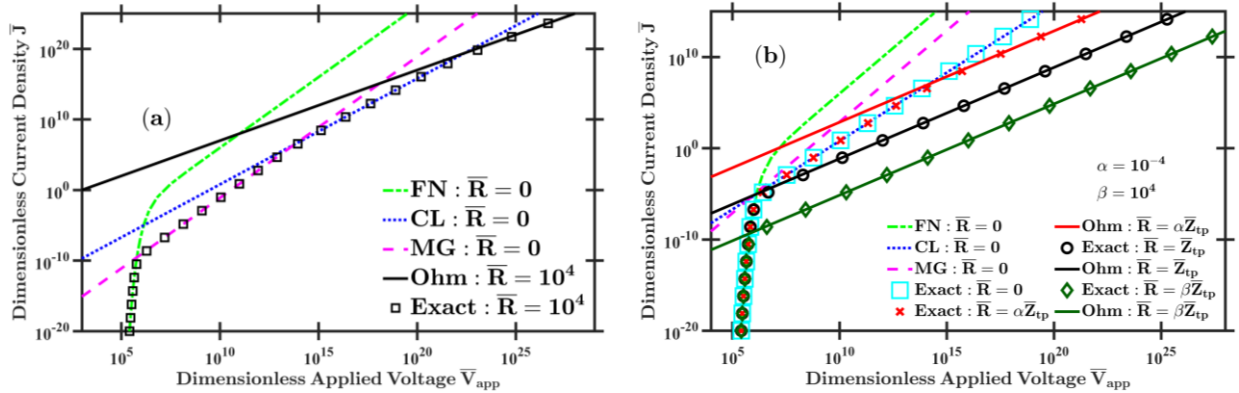


FIG. 6. Exact and asymptotic solution for dimensionless current density  $\bar{J}$  as a function of dimensionless applied voltage  $\bar{V}_{app}$  for dimensionless gap distance  $\bar{D} = 10^7$ . (a) For dimensionless electron mobility  $\bar{\mu} = 0.4843$ , electron emission transitions from Fowler-Nordheim (FN) to Mott-Gurney (MG) to Child-Langmuir (CL) for increasing  $\bar{V}_{app}$  for dimensionless resistance  $\bar{R} = 0$ . For  $\bar{R} = 10^4$ ,  $\bar{J}$  eventually follows Ohm’s Law (OL). (b) For  $\bar{\mu} = 4843$ , the asymptotic solutions for FN, MG, and CL intersect at the triple point for  $\bar{R} = 0$ . Electron emission transitions from FN to MG to CL for increasing  $\bar{V}_{app}$  for  $\bar{R} \leq \bar{Z}_{tp} = 1.38 \times 10^{11}$ , where  $\bar{Z}_{tp}$  is the gap impedance at the triple point. When  $0 \leq \bar{R} \leq \bar{Z}_{tp}$ , electron emission transitions from FN to CL to OL. When  $\bar{R} > \bar{Z}_{tp}$ , electron emission transitions directly from FN to OL [from Ref. [49]].

Figure 6a shows the transitions between the asymptotic solutions in (4)-(7) for  $\bar{D} = 10^7$ ,  $\bar{\mu} = 0.7$ , and  $\bar{R} = 10^4$  as a function of  $\bar{V}_{app}$ . The solution follows the minimum energy or minimum current principle, following the asymptotic relation giving the lowest  $\bar{V}_{app}$  at a particular  $\bar{J}$ , with modified behavior at transitions between asymptotes. At low  $\bar{J}$  and  $\bar{V}_{app}$ , the effect of the resistor is

vanishingly small upon the circuit; the opposite holds at high  $\bar{J}$  and  $\bar{V}_{app}$  when the gap becomes negligible. As before [48], gap emission behavior transitions from FN to MG to CL as  $\bar{V}_{app}$  increases; however, the external resistor causes the overall circuit to exhibit predominantly OL at very high  $\bar{J}$  and  $\bar{V}_{app}$ . While real devices operate in a much narrower range of  $\bar{J}$  and  $\bar{V}$  than depicted in Fig. 6a, Fig. 6a demonstrates the conditions for transitioning between or operating within any combination of emission conditions.

Figure 6b assesses the transitions with varying  $\bar{R}$  at constant  $\bar{\mu} = 4843$  and  $\bar{D} = 10^7$  to match triple point conditions [18]. The dimensionless impedance at the triple point is  $\bar{Z}_{tp} = 1.38 \times 10^{11}$ . To assess the influence of an external resistor, we consider  $\bar{R} = \bar{Z}_{tp}$ ,  $\bar{R} \ll \bar{Z}_{tp}$ , and  $\bar{R} \gg \bar{Z}_{tp}$ . For  $\bar{R} > \bar{Z}_{tp}$ , the behavior transitions directly from FN to OL. At  $\bar{R} = \bar{Z}_{tp}$  the FN, CL, and MG asymptotes intersect with OL, again resulting in the direct transition from FN to OL. When  $0 < \bar{R} < \bar{Z}_{tp}$ , emission transitions from FN to CL (since it passes through the triple point) to Ohm's law with the space-charge regime controllable by altering the resistance.

Practically, the resistor acts as a voltage divider. At the intersection of OL for  $R = \bar{Z}_{tp}$  and the exact solution for  $\bar{R} = 0$ , voltage is divided evenly between the circuit elements. The voltage division effect is spread over several orders of magnitude for  $\bar{V}_{app}$  and  $\bar{J}$  and varies linearly on a semi-log scale when  $\bar{R} \approx \bar{Z}_g$ . In addition, for low  $\bar{V}_{app}$  and  $\bar{J}$ ,  $\bar{V}_{app} \approx \bar{V}_g$ . These conditions facilitate conversion between  $\bar{V}_{app}$  and  $\bar{V}_g$ . Thus, the specific electron emission mechanism may be tunable by appropriate selection of applied voltage, injected current, or external resistor.

As a practical example, we apply (2) and (3) with  $A = (1.4/\varphi) \times 10^{-6+4.26/\sqrt{\varphi}}$  and  $B = 6.49 \times 10^9 \varphi^{1.5}$  [48], for  $\varphi = 4$  eV,  $\phi_0 = 6.18 \times 10^{-3}$  V,  $x_0 = 1.19 \times 10^{-13}$  m,  $J_0 = 1.27 \times 10^{17}$  A/m<sup>2</sup>,  $\mu_0 = 6.35 \times 10^{-7}$  m<sup>2</sup>/(Vs), and  $Z_0 = 1.21 \times 10^{-4}$  Ω. Choosing gap distance  $D = 250$  nm ( $\bar{D} = 2.1 \times 10^6$ ) and emission area  $S = 4 \times 10^{-16}$  m<sup>2</sup> (side length of 20 nm to avoid edge effects from finite diode),  $\bar{V}_g = 3.09 \times 10^5$  (  $V_g = 1.91$  kV),  $\bar{\mu} = 2.11 \times 10^3$  (  $\mu = 1.34 \times 10^{-3}$  m<sup>2</sup>/(Vs)), and vacuum surface field  $E = V_g/D = 7.65 \times 10^9$  V/m since we can approach the triple point from FN. At the triple point,  $J = 3.12 \times 10^{12}$  A/m<sup>2</sup> and  $I = 1.25$  mA. Defining  $v_d \equiv \mu E$  gives the electron drift velocity for this system as  $v_d = 1.02 \times 10^7$  m/s. For nitrogen,  $v_e = 3.3 \times 10^6 (E/P)^{1/2}$  where  $v_e$  and  $E$  are in cgs units and  $P$  is in Torr [58], giving  $P = 794$  Torr. This suggests that the gap acts like vacuum at any pressure below one atmosphere for these conditions. While the triple point is not directly related to the mean-free path, this gap distance is on the order of the mean-free path in air, which we recently estimated as 539 nm at 760 Torr [59]. Finally,  $\bar{Z}_{tp} = 1.26 \times 10^{10}$  ( $Z_{tp} = 1.53$  MΩ); thus, selecting  $R > 1.53$  MΩ would mask any SCLE (CL or MG) behavior in the I-V characteristics of the circuit, regardless of pressure. However, applying sufficient  $E$  to achieve the triple point in this condition may cause cathode breakdown before satisfying the triple point condition. This shows the value of the triple point as a diagnostic; an experimentalist can surmise, knowing only  $D$  and  $p$ , that this example gap will normally operate purely in the FN mode for  $V < 1.91$  kV. The triple point also predicts the conditions necessary for the existence of the MG regime; above the triple point pressure, emission will transition from FN to MG to CL, while lower pressures exhibit vacuum-like behavior over the entire spectrum of  $V$  and  $J$ . Furthermore, tuning the external resistor may allow modifying the potential difference across the gap to control electron emission behavior.

## NEXUS THEORY: INCORPORATION OF THERMIONIC WITH FIELD- AND SPACE-CHARGE LIMITED EMISSION

[A. M. Darr, C. R. Darr, and A. L. Garner, “Theoretical Assessment of Transitions across Thermionic, Field, and Space-Charge Limited Emission,” Phys. Rev. Res. **2**, 033137 (2020); A. L. Garner, G. Meng, Y. Fu, A. M. Loveless, R. S. Brayfield II, and A. M. Darr, “Transitions between electron emission and gas breakdown mechanisms across length and pressure scales,” J. Appl. Phys. **128**, 210903 (2020).]

We reported our preliminary work on the thermionic emission effort in last year’s report and attached the published paper [50] at the end of the 2021 annual report, so we will briefly summarize the key results rather than providing a detailed summary. As electron emission devices continue to push technological limits of device size, electric field, and temperature, characterization of device limitations due to thermionic (TE), field (FE), and space-charge limited emission (SCLE) becomes increasingly important for device reliability and performance. While various theoretical studies have examined the transitions between any two of these mechanisms using asymptotic nexus theory and more detailed multiphysics solutions, a full assessment across all three regimes simultaneously using a single theory remains incomplete. Using a single particle theory and the thermo-field representation of current density [20], we derived equations that recovered the asymptotic solutions for the Richardson-Laue-Dushman, Fowler-Nordheim, and Child-Langmuir laws for TE, FE, and SCLE, respectively. We observed various transitions from this full solution, including TE to FE to SCLE, the Miram curve transitioning TE to SCLE, and the discovery of a field-enhanced Miram curve. Equating two of these asymptotic solutions yielded a second order nexus; a third order nexus arises when all three asymptotic solutions match, yielding conditions for transitions from TE or FE to SCLE. We added Ohm’s law and SCLE at pressure, modeled by the Mott-Gurney law, to nexus theory, generating diode parameter phase plots showing the areas of influence for all five mechanisms. This provided additional insight into mechanistic transitions to elucidate experimental results and guide system design under more extreme design requirements.

In this report, we summarize specifically our findings with respect to varying dimensionless temperature  $\bar{T}$  and dimensionless mobility  $\bar{\mu}$ . Figure 7 shows that varying  $\bar{V}$  and  $\bar{T}$  instead of  $\bar{D}$  at fixed  $\bar{\mu} = 700$ ,  $\bar{D} = 10^7$ , and  $\bar{R} = 10^{10}$  leads to three third order nexuses within the chosen  $\bar{V} - \bar{T}$  space: FN-MG-RLD, MG-CL-RLD, and CL-OL-RLD. Using the example diode established in Fig. 7, these dimensionless parameters would be translated into the physical values  $\mu = 10^3$  cm<sup>2</sup>/(V·s) (1089 Torr),  $D = 8.5$  mm, and  $R = 810$  MΩ. The fixed parameters were chosen to enlarge each region on the phase plot; however, one could easily eliminate the MG or CL regions by modifying  $\bar{\mu}$  and/or  $\bar{R}$  – each project and device can benefit from a custom nexus phase plot if multiphysics are suspected. Relegating the influence of RLD to higher temperatures requires changing  $\bar{D}$ , the primary limiting mechanism.

The  $\bar{V} - \bar{\mu}$  parameter space is also important:  $\bar{\mu}$  varies inversely with pressure. Considering  $\bar{V}$  and  $\bar{\mu}$  in Fig. 8 at constant  $\bar{T} = 10^{-3}$ ,  $\bar{D} = 10^7$ , and  $\bar{R} = 10^6$  shows third order nexuses for FN-MG-CL and MG-CL-OL. Again, for our example diode, these are  $T = 11.6$  K,  $D = 8.5$  mm, and  $R = 81$  k $\Omega$ . This temperature would be useful for a researcher interested in cryogenics – for instance, cryogenic field emission scanning electron microscopy (cryo-FESEM), which deals with temperatures as low as 123 K [60] or 88 K [61]. With a higher work function material (say, tungsten at  $\Phi=4.5$  eV),  $\bar{T} = 10^{-3}$  becomes  $T=52.2$  K, meaning a researcher would only need to slightly adjust other parameters to make Fig. 4 relevant for cryo-FESEM. Interestingly, for the particular  $\bar{T}$  considered, RLD only intersects with FN in this parameter space; a higher  $\bar{T}$  would easily eliminate FN and make the RLD-MG and RLD-CL transitions important instead. Most individual experiments consider a much smaller subset of phase space; however, plotting a much larger space demonstrates transitions that may otherwise be neglected. For instance, in Fig. 8a researcher examining  $\bar{V} > 10^7$  and  $\bar{\mu} > 10^4$  would not encounter the FN regime, but other results demonstrate that the FN to CL nexus may influence the solution even two orders of magnitude away in  $\bar{V}$ .

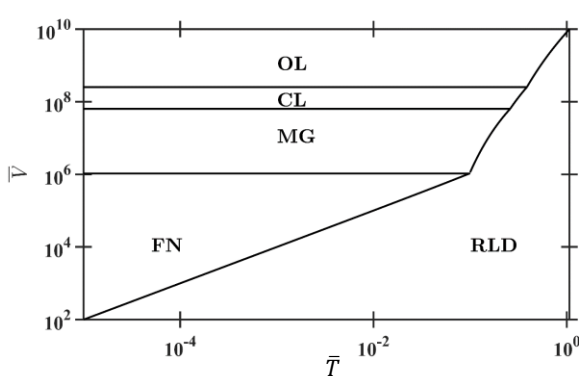


FIG. 7. Phase plot showing the conditions for various emission regimes, Ohm's law (OL), Child-Langmuir (CL), Mott-Gurney (MG), Fowler-Nordheim (FN), and Richardson-Laue-Dushman (RLD) as a function of dimensionless voltage  $\bar{V}$  and dimensionless temperature  $\bar{T}$  at fixed dimensionless electron mobility  $\bar{\mu} = 7 \times 10^2$ , dimensionless external series resistance  $\bar{R} = 10^{10}$ , and dimensionless gap distance  $\bar{D} = 10^7$ . Each black line represents a second order nexus curve between two regimes; several third order nexuses exist where lines intersect [50].

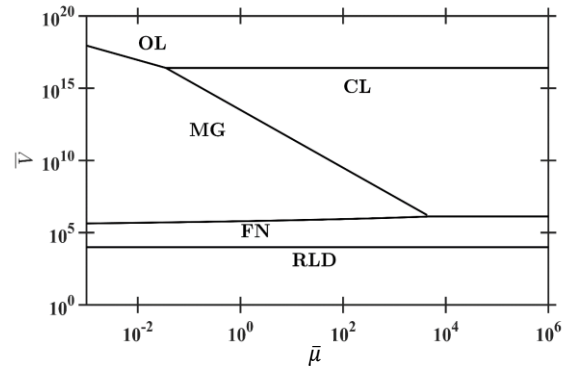


FIG. 8. Phase plot showing the conditions for various emission regimes, Ohm's law (OL), Child-Langmuir (CL), Mott-Gurney (MG), Fowler-Nordheim (FN), and Richardson-Laue-Dushman (RLD) as a function of dimensionless voltage  $\bar{V}$  and dimensionless electron mobility  $\bar{\mu}$  at fixed dimensionless gap distance  $\bar{D} = 10^7$ , dimensionless external series resistance  $\bar{R} = 10^6$ , and dimensionless temperature  $\bar{T} = 10^{-3}$ . Each black line represents a second order nexus curve between two regimes; two third order nexuses are shown where these curves intersect [50].

It is instructive to consider the critical temperature below which emission transitions solely between FN and CL. In the GTF model, emission begins to transition between thermal and field at  $T_{min} \equiv (\hbar e E) / (k_B 2\sqrt{2m\Phi} t(y))$  and becomes purely thermal at  $T_{max} = (\hbar e E) / (k_B \pi \sqrt{m\Phi} y)$  [62]. For a copper electrode with  $\Phi = 4.5$  eV,  $D = 100$  nm, and  $V = 1$  V, ignoring space-charge  $E = 10^8$  V/m,  $T_{min} = 53.3$  K, and  $T_{max} = 165.6$  K. Thus, most applications require accounting for thermionic emission to fully capture emission behavior (although the cryogenic cases mentioned above would fall within this range). At room temperature,  $T = 300$  K, the transition

from RLD to FN occurs from  $2.21 \times 10^8 \text{ V/m} < E < 5.68 \times 10^8 \text{ V/m}$ . For  $E$  above this range, emission becomes purely FE, although such high  $E$  risks damaging the cathode. These examples demonstrate the usefulness of the full theory and asymptotic solutions to an experimentalist over a wide range of  $T$  and  $E$ .

### NEXUS THEORY: INCORPORATING PHOTOEMISSION

As in prior nexus theoretical studies with planar diodes, we consider the motion of a single electron emitted from a grounded cathode with potential  $\phi = 0$  at  $x = 0$  to an anode at  $x = D$  biased to  $\phi = V$ . We can then write Poisson's equation, conservation of energy, and electron continuity as

$$\frac{d^2\phi}{dx^2} = \frac{\rho}{\epsilon_0}, \quad (4)$$

$$\frac{1}{2}mv^2 = e\phi + \frac{1}{2}mv_i^2. \quad (5)$$

and

$$J = \rho v, \quad (6)$$

respectively, where  $J$  is the current density,  $\rho$  is the charge density,  $\epsilon_0$  permittivity of free space,  $m$  is the electron mass,  $v_i$  is the initial electron velocity, and  $e$  is the elementary electron charge. Prior nexus theories have defined  $J$  as either the FN current density or the general thermal-field (GTF) emission current density when unifying SCLE with field emission or thermo/field emission, respectively. Since the objective of this study is unify SCLE, field emission, thermionic emission, and photoemission, we will replace  $J$  with the general thermal-field-photo emission (GTFP) current density, which is given by

$$J_{GTFP}(F, T) = J_p(F, T) + J_{GTF}(F, T), \quad (7)$$

where  $J_p(F, T)$  is the generalized photoemission equation [20,63], given by

$$J_p(F, T) = \frac{e}{\hbar\omega} I_{eff} P_{FD}(\hbar\omega, T), \quad (8)$$

where  $\omega = 2\pi c/\lambda$  is the angular frequency,  $\lambda$  is the wavelength,  $c$  is the speed of light in vacuum,

$$P_{FD}(\hbar\omega, T) = \frac{\left[\frac{(\hbar\omega - \phi)}{k_B T}\right]^2 + \frac{\pi^2}{6}}{\left(\frac{\mu_F}{k_B T}\right)^2 + \frac{\pi^2}{6}} \quad (9)$$

is the emission probability,

$$I_{eff} = I_i[1 - R(\theta)]F_\lambda, \quad (10)$$

$I_i$  is the initial laser intensity in units of  $\text{Wm}^{-2}$  [64-66],  $F_\lambda$  quantifies the scattering,  $R(\theta)$  is the reflectivity of a laser with incident angle  $\theta$ ,  $\hbar$  is the reduced Planck's constant,  $T$  is temperature,  $k_B$  is Boltzmann's constant,  $F$  is the electric field,  $J_p$  is the photoemission current density, and

$$J_{GTF}(F, T) = A_{RLD} T^2 N(n, s), \quad (11)$$

where  $A_{RLD} = (emk_b^2)/(2\pi^2\hbar^3)$  and  $N(n, s)$  accounts for the different regions where FE and TE occur. Similar to  $R(\theta)$ , the scattering factor  $F_\lambda$  depends on various factors, such as the incident angle; however, this is calculated using a different analytical approach [67]. Due to the complexity of  $R(\theta)$  and  $F_\lambda$ , we will treat them as constants for this analysis. For GTF,

$$N(n, s) = n \int_{-\infty}^{\infty} \frac{\ln[1 + e^{n(x-s)}]}{1 + e^x} dx \quad (12)$$

where  $n \equiv \beta_T/\beta_F$ ,  $s = \beta_F(E_m)(\hbar\omega - \varphi)$ ,  $\varphi = \Phi - \sqrt{4QF}$ ,  $Q \approx 0.36 \text{ eV nm}$ ,  $F$  is a force [20],  $\Phi$  is work function, and  $E_m = \mu_F + \varphi$ , where  $\mu_F$  is the Fermi energy, as long as the emission is below the barrier energy [68,69]. The extension to PE for the GTFP equation occurs when  $N(n, s)$  goes to  $N(n, -s)$  [20,63,69-71], given by

$$N(n, -s, u) = n \int_{-\infty}^u \frac{\ln[1 + e^{n(x+s)}]}{1 + e^x} dx, \quad (13)$$

where  $u = \beta_F(E_m)(\mu_F + \varphi - \hbar\omega)$  and  $ns = \beta_T(\hbar\omega - \varphi)$  for PE [68].

Although we have the equations necessary for the model fit, we need to determine the conditions for the PE regions to develop the asymptotic fit. transitioning to PE requires incorporating the photon energy, given by  $\hbar\omega$  [20,68], where  $\omega = 2\pi c/\lambda$ ,  $c$  is the propagation velocity of light, and  $\lambda$  is the laser wavelength. The emission regimes are specified using  $\beta_T$ ,  $\beta_F$ ,  $n$  and  $s$ . When  $n \rightarrow \infty$ ,  $J_F \rightarrow J_{FN}$ ; when  $n \rightarrow 0$ , the thermal current density goes to FN ( $J_T \rightarrow J_{RLD}$ ) [20,63,71]. Finally, when  $n^2$  goes to zero ( $n^2 \rightarrow 0$ ), the current density goes to Fowler-Dubridge (FD) ( $J_p \rightarrow J_{FD}$ ) [20,63,71]; this means that  $\beta_T$  is large. So, when  $n^2 \rightarrow 0$ , the second half of (2.9) will go to zero leaving  $J_p$ .

Such equations may be modified by incorporating mobility or resistance to include more physical phenomena. Alternatively, we may apply nexus theory to assess the necessity of deriving such full solutions or applying the appropriate asymptotic representations for MG for SCLE with collisions or Ohm's law for high resistance. The current study focuses on incorporating photoemission into the previous studying linking the GTF theory with SCLE, so we choose to replace the GTF theory with GTFP to incorporate photoemission into the full theory here and then match the relevant asymptotic solutions for the other phenomena. In the case where the Fowler-Nordheim current density  $J_{FN}$  was used to assess nexus theory,  $J \rightarrow J_{FN}$  as  $V \rightarrow 0$ ; using GTF,  $J \rightarrow J_{RLD}$  at low  $V$  and high  $T$ ; using GTFP, we anticipate  $J \rightarrow J_{FD}$   $F \rightarrow 0$  and  $T \rightarrow 0$ , where  $J_{FD}$  is the Fowler-Dubridge current density, given by

$$J_{FD}(F, T) = \left(\frac{e}{\hbar\omega}\right) I_{eff} P_{FD}(\hbar\omega, T). \quad (14)$$

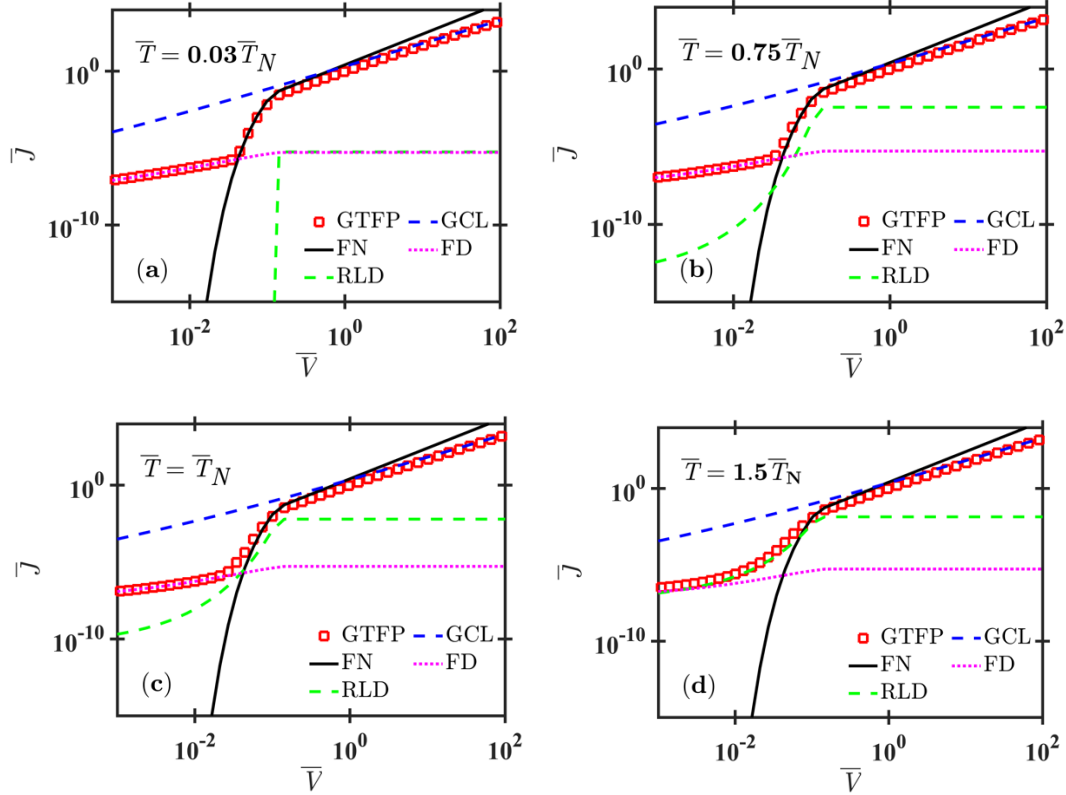


FIG. 9. Dimensionless current density  $\bar{J}$  as a function of the nondimensional voltage  $\bar{V}$  for the full solution (GTFP) and asymptotic limits for GCL (blue), FN (black), RLD (green), and FD (magenta) for different variations of the nexus temperature (a) 82.5 K ( $0.03\bar{T}_N$ ), (b) 2062.5 K ( $0.75\bar{T}_N$ ), (c) 2750 K ( $\bar{T}_N$ ), and (d) 4125 K ( $1.5\bar{T}_N$ ) for a nexus temperature of  $T_N = 2750$  K ( $\bar{T}_N = 0.0527$ ). The third order nexus between FD, FN, and RLD can be seen at the nondimensionalized temperature. These plots are for a copper cathode with  $D = 1$  nm,  $F_\lambda = R(\theta) = 0.5$ ,  $\lambda = 266$  nm ( $\hbar\omega = 4.66$  eV), and  $I_i = 3.2 \times 10^{11}$  W m $^{-2}$ . [from Ref. [50]].

After following a similar nondimensionalization scheme as reported elsewhere, Fig. 9 shows  $\bar{J}$  as a function of  $\bar{V}$  to demonstrate the transition in emission mechanism for a copper cathode with  $D = 1$  nm,  $\lambda = 266$  nm ( $\hbar\omega = 4.66$  eV),  $I_i = 3.2 \times 10^{11}$  W m $^{-2}$ , and  $F_\lambda = R(\theta) = 0.5$  for  $0.03\bar{T}_N \leq \bar{T} \leq 1.5\bar{T}_N$  ( $2750$  K  $\leq T \leq 4125$  K). These figures include the transitions between GTFP, FD, FN, GCL, and RLD. Each of these temperatures provides information about potential operating temperatures for experiments and electronic devices. With the lower temperature, (a) 82.5 K ( $0.03\bar{T}_N$ ), RLD does not interact with the other asymptotic limits. As the temperature increases RLD has a closer transition with the other asymptotic limits; RLD transitions between GCL, GTFP, and FN at a higher current density. While FD, RLD, GTFP, and FN connect at a nexus point. This is expected due to the conditions under which GCL occurs. We are currently working to finalize nexus curves similar to what we reported above for thermionic emission, which becomes complicated due to the various dependences introduced when considering photoemission. We are also working to finalize a manuscript to submit to a special issue of the *Journal of Vacuum Science and Technology B*.

## LIQUID EMISSION

[S. A. Lang, A. M. Darr, and A. L. Garner, “Theoretical analysis of the transition from field emission to space-charge-limited emission in liquids and gases,” *J. Appl. Phys.* **128**, 185104 (2020).]

Our Year 2 report outlined our preliminary work on applying nexus theory to liquids, which fewer studies have characterized [72-78]. Broadly speaking, characterizing electron processes in dielectric liquids has implications in multiple areas, including radiation physics/chemistry, field induced polymerization, nuclear radiation detection, medical imaging, insulator physics, composite insulation, high power capacitors, pulsed power systems, and electrostatics generators [77]. The characterization of electron processes in liquids includes understanding electron emission (field emission in particular) as one of the initial phases in the development of electronic breakdown [79-81]; the electron emission at the cathode initiates the release of electrons that leads to breakdown [80,81].

Phenomenologically, characterizing electron emission in liquids is important for understanding breakdown, or plasma formation, in liquids. Electron emission in liquids is potentially relevant in multiple applications, such as electric pulse applications in medicine and sterilization [82], plasma treatments of liquids for food and water decontamination [83,84], combustion [85,86], and field emission electric propulsion for flexible propulsion of satellites [87,88]. While many of these applications have grown in importance over the past two decades, many of the pertinent investigations in electron emission in liquids occurred over thirty years ago, motivating the present study to revisit the mechanistic behavior of this phenomenon.

Basically, the theory that we derived earlier for gases with collisions unifying Fowler-Nordheim, Mott-Gurney, and Child-Langmuir should be equally valid for liquids. Bragg, *et al.* described phenomena concerning electron transport, inhomogeneous electric field, SCL emission, and breakdown in a liquid, which resemble the description above for a gas with collisions [48]. Halpern and Gomer carried out the first measurements of field emission in liquid H<sub>2</sub>, D<sub>2</sub>, He, benzene, O<sub>2</sub>, and Ar, demonstrating FN-scaling at lower currents and SCL emission at higher currents [73-75], similar to the theoretical [48] and experimental observations [89] for gases. These studies showed that He and Ar transitioned to SCL emission, abruptly leading to electron avalanching with concomitant gas-bubble formation at the tip. This gas-bubble formation, which is also important in water purification [84], was a pre-breakdown phenomenon. Dotoku, *et al.* measured FE in n-Hexane, trimethylpentane (TMP), and tetramethylsilane (TMS) [90]. They observed a transition from FE to SCLE for these nonpolar liquids and that SCLE in liquids was more dominant than SCLE in vacuum due to the charge carrier velocity in liquids [90]. We will focus our study on these nonpolar liquids to demonstrate the utility of our approach; such a process may ultimately be extended to other liquids [73-75].

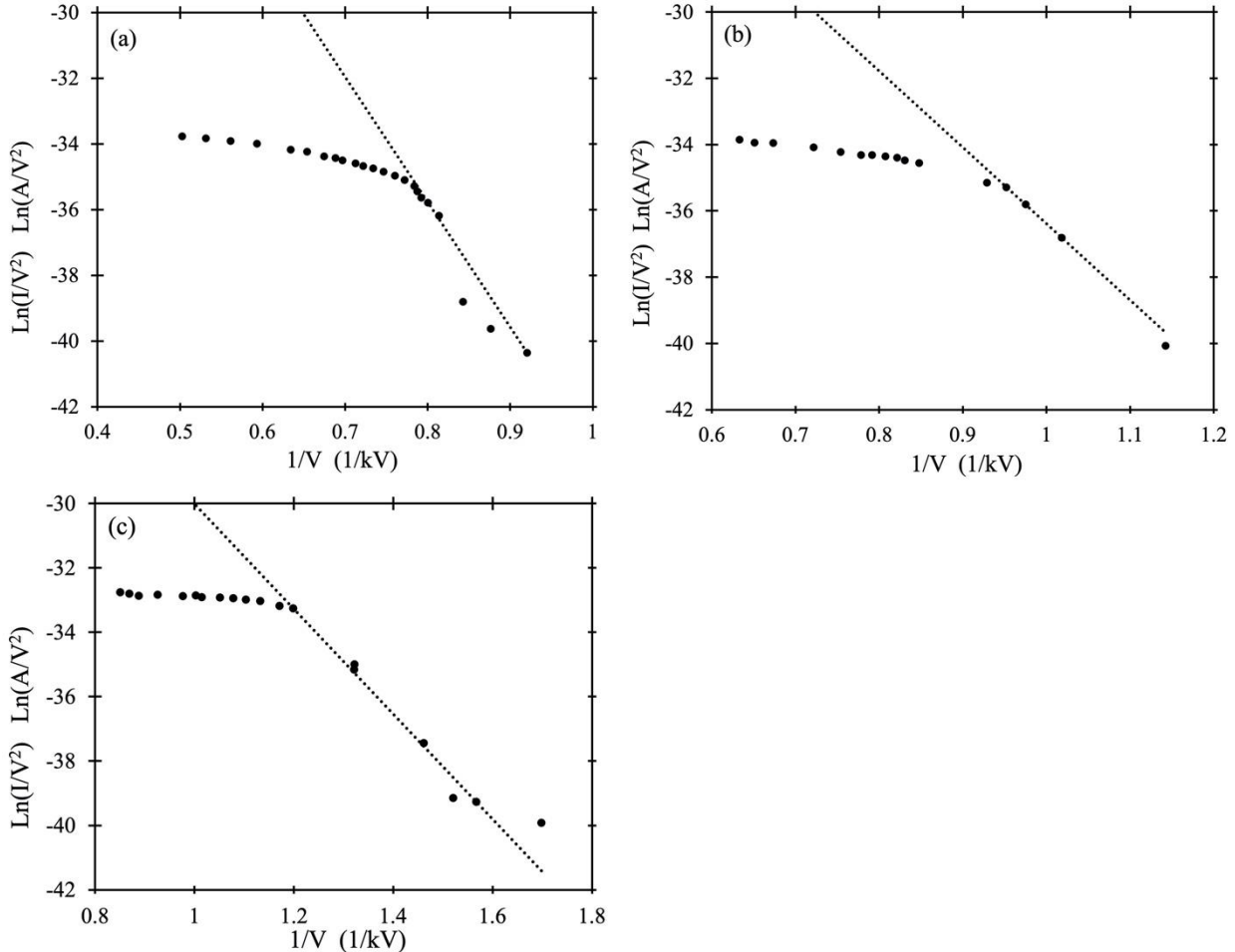


FIG 10. Experimental data (from Fig. 5 of Ref. [90] filled circles) on a Fowler-Nordheim (FN) plot of  $\ln(I/V^2)$  as a function of  $1/V$  and the best-fit lines (dotted lines) using (14) to determine the modified FN coefficients  $A'_{FN}$  and  $B'_{FN}$  for (a) n-Hexane, (b) TMS, and (c) TMP. [from Ref. [91]]

Plotting the experimental data [91] on a FN plot yields the modified FN constants  $A'_{FN}$  and  $B'_{FN}$  from the best fit lines shown in Fig. 6 for n-Hexane, TMP, and TMS.

Figure 11 shows the final nondimensionalized current density  $\bar{J}$  as a function of  $\bar{V}$ . As observed for gases [48], the exact solution follows the FN law at lower  $\bar{V}$  and transitions to the MG law with increasing  $\bar{V}$ . The liquids and experimental conditions considered here generally remain in the FN regime and only begin to transition to the SCL regime, characterized by MG for liquids, rather than reaching the asymptotic solution. As anticipated, we do not observe a transition to CL, which may occur for vacuum.

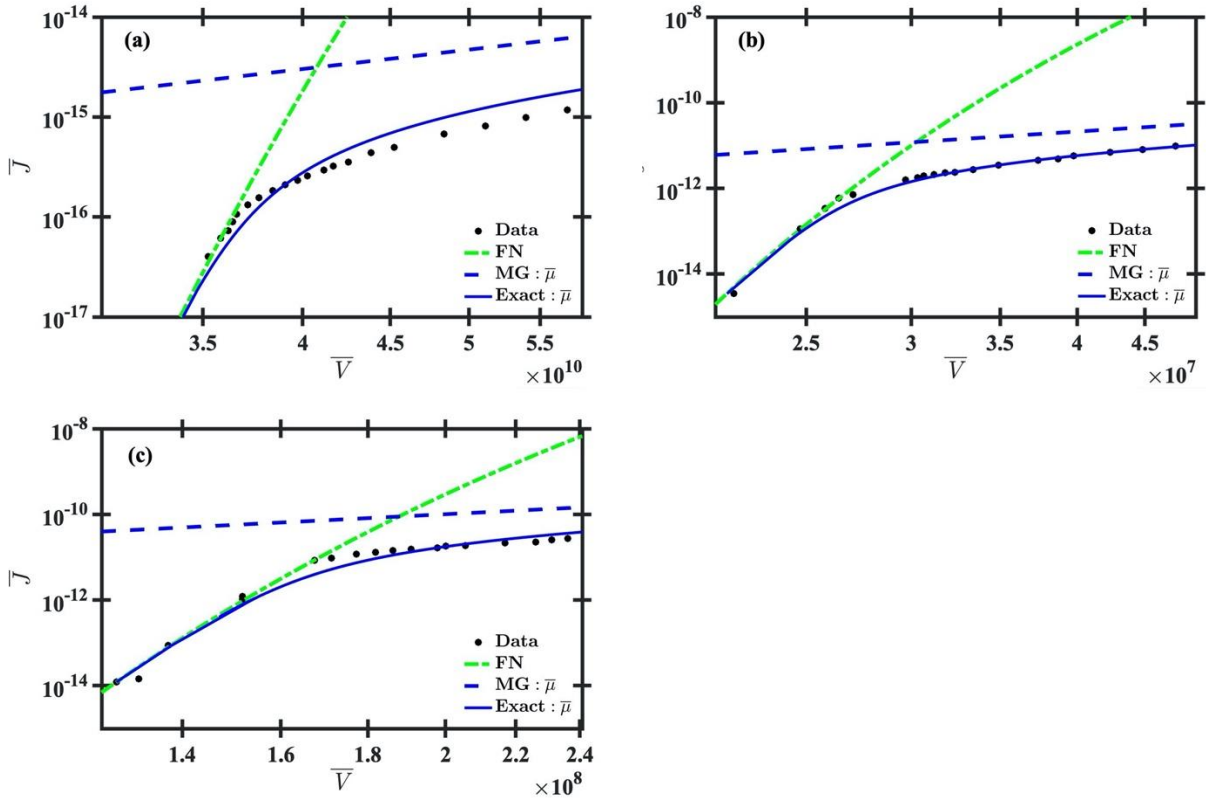


FIG. 11. Nondimensional current density  $\bar{J}$  as a function of nondimensional applied voltage  $\bar{V}$  showing the experimental data [90], exact solution, and asymptotic solutions of Fowler-Nordheim (FN) and Mott-Gurney (MG) for (a) n-Hexane, (b) TMP, and (c) TMS. The best fit exact solution agrees well with the experimental data over the full range of measurements for each liquid once in the field emission regime [from Ref. [91]].

We selected the n-hexane data as the baseline for  $\bar{\mu}$  and  $\bar{d}$  for a liquid and fix  $\bar{d} = 1.0931 \times 10^{12}$  increasing and decreasing  $\bar{\mu}$  by two orders of magnitude to explore the range that may encompass phase change. Note that although we chose n-hexane as the baseline, carrying out this analysis using these dimensionless variables makes this assessment universal, or true for any substance under appropriate conditions to yield the same dimensionless conditions. Figure 12 shows the exact solution and the asymptotes for FN, MG, and CL for  $\bar{\mu} = 2.19 \times 10^{-2}, 2.19 \times 10^0$ , and  $2.19 \times 10^2$  to capture this range of behavior. Our prior studies indicated that increasing  $\bar{\mu}$  causes  $\bar{J} \rightarrow \bar{J}_{CL}$  with increasing  $\bar{V}$  while  $\bar{J} \rightarrow \bar{J}_{MG}$  at lower  $\bar{\mu}$ . Figure 13 shows that increasing  $\bar{\mu}$  to  $2.19 \times 10^2$  causes  $\bar{J}$  to rapidly approach  $\bar{J}_{CL}$ , while both from  $\bar{\mu} = 2.19 \times 10^{-2}$  and  $\bar{\mu} = 2.19 \times 10^0$  approach  $\bar{J}_{MG}$  at much higher  $\bar{V}$  than plotted here. From a practical perspective, the experimental data for n-Hexane at  $\bar{\mu} = 2.19 \times 10^0$  followed FN up to  $\bar{V} \approx 10^{11}$  before beginning to approach MG. These results suggest that increasing  $\bar{\mu}$  by two orders of magnitude, loosely corresponding to a transition to a gaseous state, is not sufficient to induce electron emission to transition to CL for the present design, particularly  $\bar{d}$ . However, it suggests that adjusting  $\bar{d}$  may make it feasible for electron emission to transition from FN to MG to CL with a phase change.

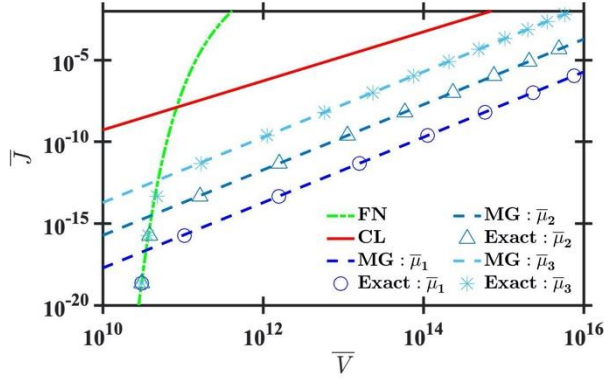


FIG. 12. Universal curves for current density  $\bar{J}$  as a function of  $\bar{V}$  for various  $\bar{\mu}$  with  $\bar{\mu}_2 = 2.19 \times 10^0$  selected as the baseline based on the n-hexane measurements and asymptotic solutions for Fowler-Nordheim (FN), Mott-Gurney (MG), and Child-Langmuir (CL). We consider  $\bar{\mu}_1 = 2.19 \times 10^{-2}$ ,  $\bar{\mu}_2 = 2.19 \times 10^0$ , and  $\bar{\mu}_3 = 2.19 \times 10^2$  to account for  $\bar{\mu}$  that may correspond to a phase change from liquid to dense vapor or gas [from Ref. [91]].

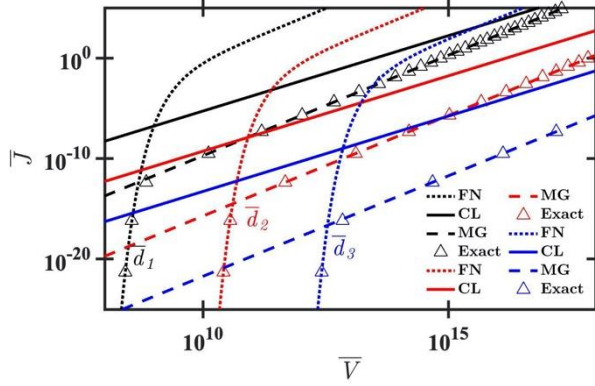


FIG. 13. Universal curves for nondimensional current density  $\bar{J}$  as a function of nondimensional applied voltage  $\bar{V}$  showing asymptotic solutions for Fowler-Nordheim (FN), Mott-Gurney (MG), and Child-Langmuir (CL) asymptotic solutions, and the exact solutions for  $\bar{d}_1 = 1.0931 \times 10^{10}$  (black),  $\bar{d}_2 = 1.0931 \times 10^{12}$  (red), and  $\bar{d}_3 = 1.0931 \times 10^{14}$  (blue). Decreasing  $\bar{d}$  causes electron emission to more quickly transition from FN to MG. Reaching CL requires a much higher  $\bar{V}$  than used experimentally, even for the smaller gap size. Increasing  $\bar{d}$  necessitates a very large  $\bar{V}$  to achieve MG, making it much more likely for electron emission to remain characterized by FN [from Ref. [91]]..

Based on our prior observations on the impact of gap distance on emission for gases [48], we anticipate that changing  $\bar{d}$  should also influence the emission mechanism. Considering our baseline case for n-Hexane of  $\bar{\mu} = 2.19 \times 10^0$  and  $\bar{d} = 1.0931 \times 10^{12}$ , we assess the impact of  $\bar{d}$  on electron emission by decreasing and increasing  $\bar{d}$  by an order of magnitude to  $1.0931 \times 10^{10}$  and  $1.0931 \times 10^{14}$ , respectively. Setting  $\bar{d} = 1.0931 \times 10^{14}$  necessitates a very large  $\bar{V}$  before space charge influences emission. Reducing  $\bar{d}$  to  $1.0931 \times 10^{10}$  leads to a rapid transition from FN to MG, as well as the potential to approach CL at a  $\bar{V}$  that may potentially be feasible. These results, shown in Fig. 9, suggest that the influence of space charge to emission in liquids is very sensitive to gap distance. Although it seems unlikely that one would approach CL for a liquid before other effects of strong electric field may become dominant, these results suggest that reducing the gap size by an order of magnitude for n-hexane would clearly lead to emission

becoming dominated by space charge through MG very quickly with increasing voltage. These results also indicate that liquids that may yield similar nondimensional parameters may achieve CL, although the likelihood of this occurring requires further study.

## NEXUS THEORY: LINKING ELECTRON EMISSION AND BREAKDOWN EMISSIONS FROM QUANTUM SCALE TO PASCHEN'S LAW

[A. M. Loveless, A. M. Darr, and A. L. Garner, “Linkage of Electron Emission and Breakdown Mechanism Theories from Quantum Scales to Paschen’s Law,” *Phys. Plasmas* **28**, 042110 (2021).]

We defined a common set of scaling parameters across the range of dominant mechanisms to derive a theory linking electron emission and breakdown mechanism theories from quantum scales to Paschen’s law to obtain asymptotic solutions for quantum space-charge limited emission (QSCL), classical space-charge limited emission (CSCL), space-charge limited emission with collisions (MG), Fowler-Nordheim field emission (FN), field emission driven gas breakdown, and classical gas breakdown defined by Paschen’s law (PL) [92]. These non-dimensionalized equations are universal (true for any gas) across all regimes except for PL, which contains a single, material-dependent parameter. Figure 14 shows a plot of the current density as a function of voltage demonstrating the transitions between multiple mechanisms, such as QSCL to CSCL, CSCL to FN, CSCL to MG to FN. Figure 15 shows a nexus plot demonstrating the transitions between these emission mechanisms.

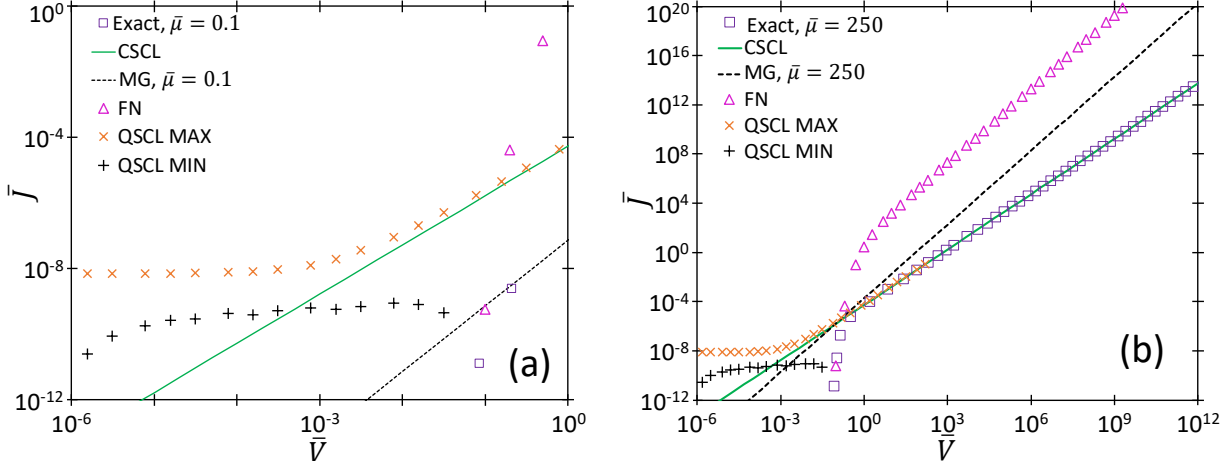


FIG. 14. Dimensionless current density  $\bar{J}$  as a function of dimensionless applied voltage  $\bar{V}$  for a 10 nm gap demonstrating the transitions of the exact solution obtained by numerically solving (10)-(12) to the numerical solution of (9) for QSCL and the exact analytic solutions for CSCL (13), FN (14), and MG (15) focusing on (a) the transition from QSCL to CSCL and (b) the full spectrum of transitions. We consider the minimum (QSCL MIN) solution as the relevant solution until the transition to CSCL [from Ref. [92]].

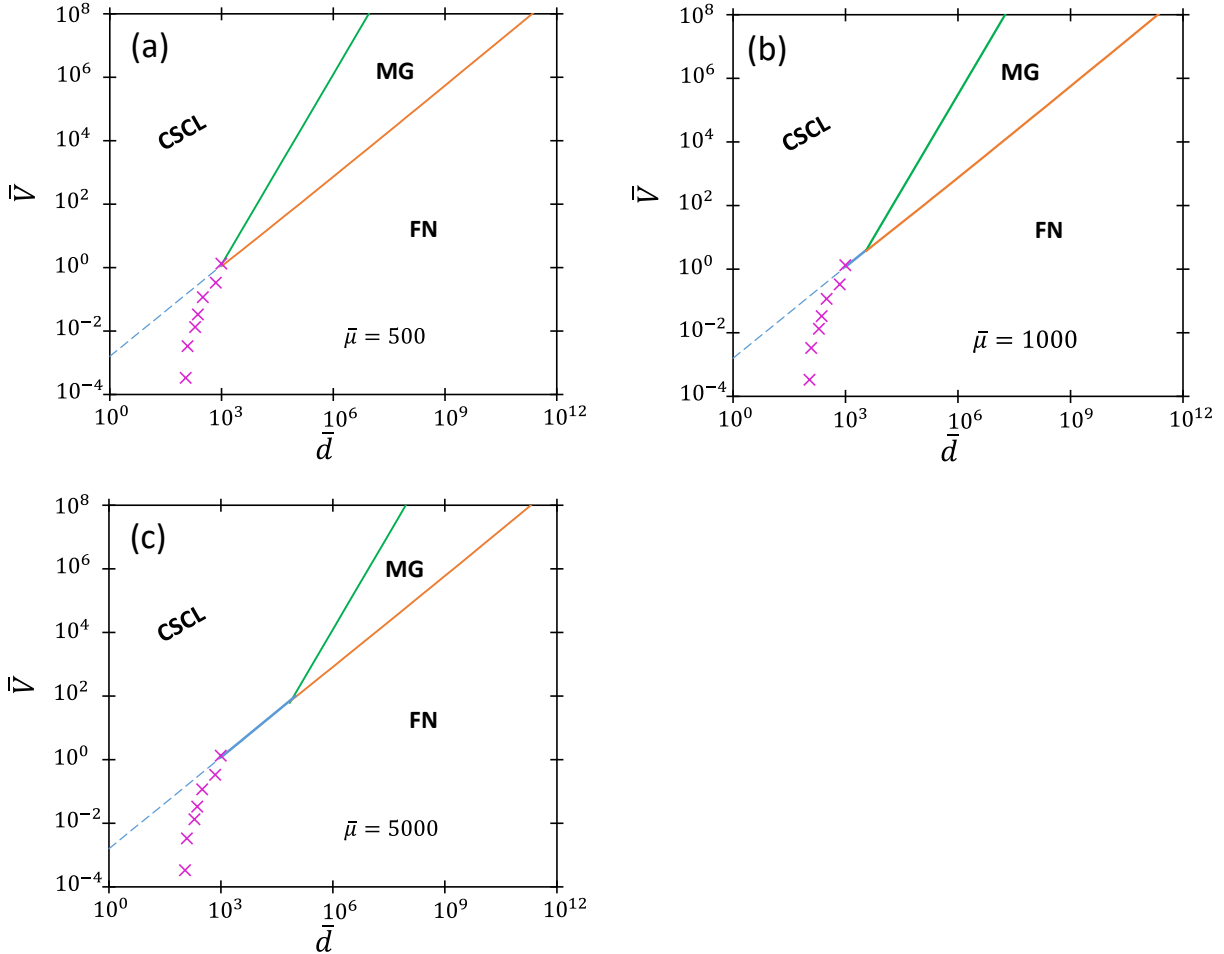


FIG. 15. Dimensionless applied voltage  $\bar{V}$  as a function of dimensionless gap distance  $\bar{d}$  demonstrating the respective regions where each emission mechanism should dominate for dimensionless mobilities of (a)  $\bar{\mu} = 500$ , (b)  $\bar{\mu} = 1000$ , and (c)  $\bar{\mu} = 5000$ . The dashed line denotes the continuation of the nexus between the classical Child-Langmuir law (CSCL) and the Fowler-Nordheim (FN) law. The “x” symbols denote the numerical results of the contribution due to quantum effects (QSCL) using the QSCL MIN shown in Fig. 6, which shifts the transition from FN to space-charge limited emission to lower  $\bar{V}$ . In this case, (a) denotes a fourth order nexus between QSCL, CSCL, MG, and FN [from Ref. [92]].

This theory is fully universal (independent of gas and electrodes) from QSCL to FN; it can be linked with field emission driven breakdown and, eventually to Paschen’s law (with one material dependent constant remaining Paschen’s law). Although the theory is not fully unified, it used a single non-dimensionalization scheme that can facilitate experimental designs concerned with crossing these regimes. Furthermore, we demonstrated the conditions for more complicated nexuses, such as matching QSCL, CSCL, MG, and FN. This provided valuable information to experimentalists concerning regimes where slight perturbations in conditions may alter the electron emission mechanism and to theorists concerning the applicability of the asymptotic solutions or reduced nexus theories.

## 1-D SPACE-CHARGE LIMITED CURRENT USING CONFORMAL MAPPING

[N. R. Sree Harsha and A. L. Garner, “Applying Conformal Mapping to Derive Analytical Solutions of Space-Charge-Limited Current Density for Various Geometries,” IEEE Trans. Electron Devices **68**, 264-270 (2021).]

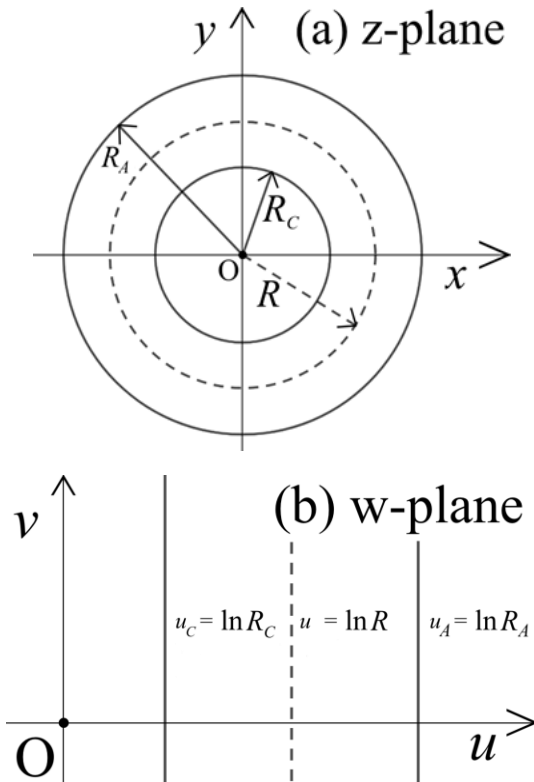


FIG. 16. (a) A cross-section of two infinite concentric cylinders in the *z*-plane. (b) The annular region between the circles in the *z*-plane is mapped one-to-one and onto the region between the two lines in the *w*-plane [52].

determine the appropriate relationships for more complicated geometries.

We first consider a cathode and an anode as two concentric cylinders of infinite length with radii  $R_C$  and  $R_A$ , respectively, as shown in Fig. 16(a). The cross-sections of these cylinders can be represented in the complex *z*-plane by  $z = Re^{i\theta}$ . The transformation  $w = f(z) = \ln z$  maps the circles into lines in the *w*-plane, as shown in Fig. 16(b) [93]. Applying the 1-D representation of  $\phi$  to the *w*-plane yields

$$\phi = \frac{V(u - u_C)^{4/3}}{(u_A - u_C)^{4/3}}. \quad (15)$$

Transforming (15) into the *z*-plane gives the potential in the *z*-plane as

While exact analytic solutions for space-charge-limited current (SCLC) are well established for parallel plate geometries, they have only recently been derived for concentric cylindrical and spherical geometries using variational calculus. However, actual diode systems and slow wave structures are usually more complicated, making SCLC calculations more difficult. Thus, we applied conformal mapping to derive the analytical solutions for SCLC for various complicated geometries exhibiting curvilinear flow [52]. We first replicated the exact solution of SCLC for concentric cylindrical electrodes from variational calculus by using conformal mapping to transform from the Child-Langmuir (CL) law for a planar geometry. We then derived SCLC in other geometries by using conformal transformations to either the planar or concentric cylinder solution. Because the SCLC calculated using such conformal mappings depends only on the CL law, this may permit future incorporation of relativistic or quantum corrections to

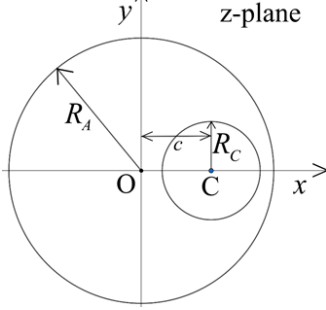
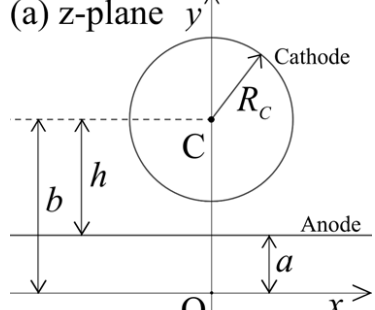
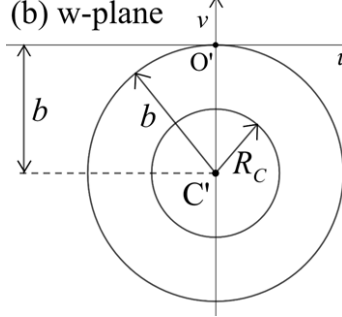
$$\phi = V \frac{(\ln R - \ln R_C)^{4/3}}{(\ln R_A - \ln R_C)^{4/3}} = V \left[ \frac{\ln(R/R_C)}{\ln(R_A/R_C)} \right]^{4/3}. \quad (16)$$

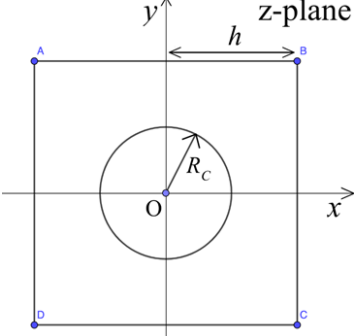
Substituting (16) into Poisson's equation and applying the Laplacian in cylindrical coordinates yields the SCL current density near the cathode for cylindrical coordinates as

$$J_{\text{SCL}} = \frac{4}{9} \epsilon_0 \sqrt{\frac{2e}{m}} \frac{V^{3/2}}{R_C^2 [\ln(R_A/R_C)]^2}, \quad (17)$$

which agrees with the result from variational calculus [53]. Table I summarizes the results for other geometries considered.

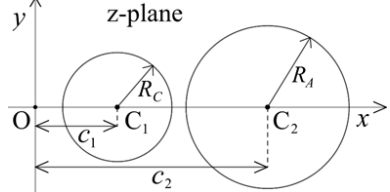
TABLE I: Summary of results using conformal mapping to calculate space-charge limited current [52].

 <p>A cross-section of eccentric cylinders with anode of radius <math>R_A</math> and cathode of radius <math>R_C</math> and a displacement <math>c</math> between their centers in the <math>z</math>-plane.</p> $J_{\text{SCL}} \approx \frac{4\epsilon_0}{9} \sqrt{\frac{2e}{m}} \frac{V^{3/2}}{R_C^2 \left( \cosh^{-1} \frac{(R_A^2 + R_C^2 - c^2)}{2R_C R_A} \right)^2}.$	<p>(a) <math>z</math>-plane </p> <p>(b) <math>w</math>-plane </p> <p>(a) A cross-section in <math>z</math>-plane of infinite plane as the anode placed at a distance <math>h</math> from the center of the cylindrical cathode <math>C</math> of radius <math>R_C</math> such that <math>R_C \ll h</math>. (b) The anode and the cathode are transformed into two concentric circles centered at <math>C'</math> in the <math>w</math>-plane.</p> $J_{\text{SCL}} \approx \frac{4\epsilon_0}{9} \sqrt{\frac{2e}{m}} \frac{V^{3/2}}{R_C^2 \left( \ln \left[ \left( h + \sqrt{h^2 - R_C^2} \right) / R_C \right] \right)^2}$
---	---



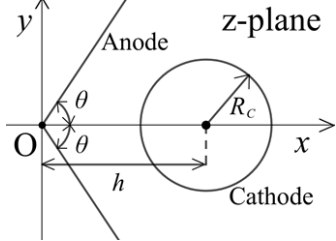
A cross-section of a doubly connected region consisting of a cylindrical cathode centered inside a square anode. The anode may be mapped onto an annulus using a numerical transformation approximation.

$$J_{SCL} \approx \frac{4}{9} \epsilon_0 \sqrt{\frac{2e}{m}} \frac{V^{3/2}}{R_c^2 [\ln(1.08h/R_c)]^2}.$$



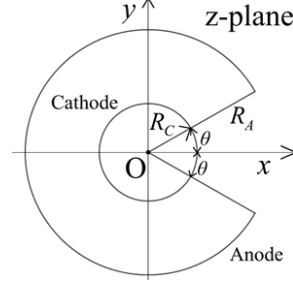
A cross-section of two external cylinders in the  $z$ -plane mapped onto an annulus centered at the origin in the  $w$ -plane by using fractional linear transformation.

$$J_{SCL} \approx \frac{4\epsilon_0 \sqrt{2e}}{9\sqrt{m}} \frac{V^{3/2}}{R_c^2 \left( \ln \frac{R_A}{R_C} + \ln \frac{c_1 + \sqrt{c_1^2 - R_C^2}}{c_2 + \sqrt{c_2^2 - R_A^2}} \right)^2}$$



A cross-section of two 1-D planar anodes intersecting at an angle  $2\theta$  at the origin and a cylindrical cathode of radius  $R_C$  at a distance  $h$  from the  $y$ -axis.

$$J_{SCL} \approx \frac{16\theta^2 \epsilon_0}{9\pi^2} \sqrt{\frac{2e}{m}} \frac{V^{3/2}}{R_c^2 (\ln [2(h/R_c)^{2\theta/\pi}])^2}.$$



A cross-section of a concentric slotted diode consisting of a slotted anode of radius  $R_A$ , and an unslotted cathode of radius  $R_C$ , and a slot represented by angle  $2\theta$ .

$$J_{SCL} \approx \frac{4}{9} \epsilon_0 \sqrt{\frac{2e}{m}} \frac{V^{3/2}}{R_c^2 (\ln [R_A/R_c])^2}$$

## 2-D AND 3-D CHILD-LANMUIR LAW

While prior theoretical studies of multi-dimensional space-charge-limited current (SCLC) assumed emission from a small patch in infinite electrodes, none have considered the more practical geometry in which the size of the emission area is on the same order of magnitude as the emitter. We apply variational calculus (VC) and conformal mapping, which have previously been used to derive analytic solutions for SCLC for non-planar geometries, to obtain mathematical relationships for general, multi-dimensional geometries. We first derive a mathematical relationship between space-charge-limited potential and vacuum potential for a general diode and derive SCLC density for an eccentric spherical diode. We then apply VC and the Schwartz-Christoffel transformation to derive an exact analytic solution for a generalized two-dimensional planar geometry that reduces to the prior finite emitting patch for infinite electrodes to first order approximation. After generalizing this approach to determine SCLC density for any orthogonal diode by using the vacuum capacitance, we present an accurate analytical formulation of three-dimensional (3-D) CL law for parallel plate diodes with rectangular and disk geometries. These

results demonstrate the utility for calculating SCLC for any geometry to guide experiment and simulation development.

Defining the dimensionless quantity  $\bar{\phi} = \phi/V_g$  gives the potential in a space-charge limited diode with any geometry as

$$\overline{\phi_{\text{SCL}}} = \overline{\phi_0}^{4/3}, \quad (18)$$

such that the spatial profile of the electric potential of a space-charge-limited diode may be calculated directly from the vacuum potential with the 4/3-power dependence independent of geometry. Since  $\phi_{\text{SCL}}$  satisfies the Poisson's equation with  $\rho_{\text{SCL}}$  as the volumetric space charge density, given by  $\nabla^2 \phi_{\text{SCL}} = \rho_{\text{SCL}}/\epsilon_0$ , the analytic solution of  $\phi_{\text{SCL}}$  for many diode geometries is not always possible [94]; however, the vacuum potential distribution can be easily obtained by solving the Laplace equation, given by  $\nabla^2 \phi_0 = 0$ . Equation (18) thus provides an easy way to determine  $\phi_{\text{SCL}}$  from  $\phi_0$  for *any* geometry and determine  $J_{\text{SCL}}$ , as illustrated in the next section.

We now use the relationship between the space-charge-limited potential and the vacuum potential to formulate SCLC density in terms of the vacuum capacitance for a 2-D planar geometry with finite electrodes. Combining Poisson's equation and the electron force law gives the SCLC density for any diode geometry as

$$J_{\text{SCL}} = \frac{\epsilon_0}{4} \sqrt{\frac{2e}{m_e}} \frac{|\nabla \phi_{\text{SCL}}|^2}{\sqrt{\phi_{\text{SCL}}}}. \quad (19)$$

Applying  $\overline{\phi_{\text{SCL}}} = \phi_{\text{SCL}}/V_g$ , we can recast (19) as

$$J_{\text{SCL}} = \frac{\epsilon_0 V_g^{3/2}}{4} \sqrt{\frac{2e}{m_e}} \frac{|\nabla \overline{\phi_{\text{SCL}}}|^2}{\overline{\phi_{\text{SCL}}}^{1/2}}. \quad (20)$$

Combining (18) and (20) yields

$$J_{\text{SCL}} = \frac{\epsilon_0 V_g^{3/2}}{4} \sqrt{\frac{2e}{m_e}} \frac{|\nabla \overline{\phi_0}^{4/3}|^2}{\overline{\phi_0}^{2/3}}. \quad (21)$$

We also have

$$|\nabla \overline{\phi_0}^{4/3}|^2 = \frac{16 \overline{\phi_0}^{2/3}}{9} \sum_{i=1}^3 \frac{1}{h_i^2} \left( \frac{\partial \overline{\phi_0}}{\partial q_i} \right)^2 = \frac{16 \overline{\phi_0}^{2/3}}{9} |\nabla \overline{\phi_0}|^2, \quad (22)$$

which we can combine with (21) to obtain the relationship between the SCLC density and the vacuum electric field as

$$J_{\text{SCL}} = \frac{4\epsilon}{9} \sqrt{\frac{2e}{m_e}} V_g^{3/2} |\nabla \phi_0|^2. \quad (23)$$

We shall now consider an infinite parallel plate geometry where the anode and the cathode are infinite planes separated by a distance  $D$  with the anode held at  $\phi(D) = V_g$  and the cathode held at  $\phi(0) = 0$ . Since  $J_{1D}$  represents the steady state current density,  $J_{\text{SCL}}$  near the cathode for this parallel plate geometry can be derived by taking volume average of (23). Defining  $V$  as the total volume in the diode gap and  $dV = dx dy dz$  as the infinitesimal volume allows us to rewrite (23) as

$$J_{\text{SCL}} = \frac{4\epsilon_0}{9} \sqrt{\frac{2e}{m_e}} V_g^{3/2} \frac{\int_0^V |\nabla \phi_0|^2 dV}{\int_0^V dV}. \quad (24)$$

Since the system's vacuum capacitance is given by  $C_0 = \epsilon_0 \int_0^V |\nabla \phi_0|^2 dV$  [95], we can write (24) as

$$J_{\text{SCL}} = \frac{4}{9} \sqrt{\frac{2e}{m_e}} V_g^{3/2} \frac{C_0}{\int_0^V dV}. \quad (25)$$

Substituting the vacuum capacitance for this 1-D diode, given by  $C_0 = \epsilon_0 WL/D$ , in (25) and noting that the total volume is  $\int_0^V dV = WLD$  recovers the familiar 1-D CL law.

For the 2-D CL law, we consider a pair of parallel planes of length  $W$ , separated by a distance  $D$ , as shown in Fig. 17. Note that these planes are finite in the direction of length (the  $x$ -axis) and infinite in depth (the  $y$ -axis). Palmer applied the Schwartz-Christoffel transformation to determine the vacuum capacitance, including all the effects of the fringing fields, of such a system [96]. Assuming modulus  $m \in (0,1)$  and a corresponding complementary modulus  $\mu \equiv \sqrt{1 - m^2}$ , allows the construction of an argument  $\omega$  using

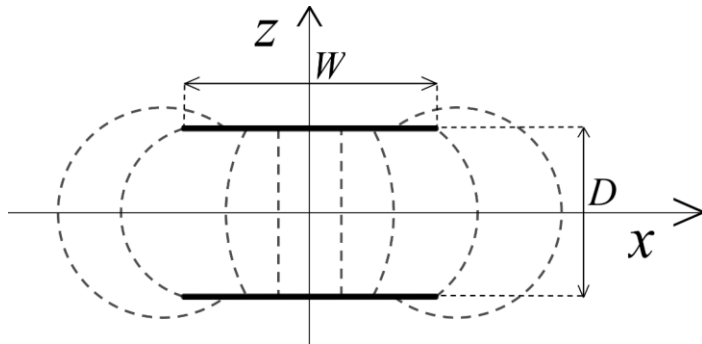


FIG. 17. The cross-section of the diode geometry for the 2-D CL law shown in  $x$ - $z$  plane. A few of the fringing fields from the anode, positioned at  $z = D/2$ , to the cathode at  $z = -D/2$  are approximately shown by longer dashed lines.

$$\sin^2 \omega = \frac{F\left(\frac{\pi}{2}, \mu\right) - E\left(\frac{\pi}{2}, \mu\right)}{\mu^2 F\left(\frac{\pi}{2}, \mu\right)}, \quad (26)$$

where  $F(\pi/2, \mu)$  and  $E(\pi/2, \mu)$  are the complete elliptic integrals of first and second kind with  $F(\theta, \mu) = \int_0^\theta dt / \sqrt{1 - \mu^2 \sin^2 t}$  and  $E(\theta, \mu) = \int_0^\theta \sqrt{1 - \mu^2 \sin^2 t} dt$  as the incomplete elliptic integrals of the first and second kind, respectively [97]. The values  $m$ ,  $\mu$  and  $\omega$  are then used to obtain the ratio of  $W/D$  using

$$\frac{W}{D} = \frac{F\left(\frac{\pi}{2}, \mu\right)E(\omega, \mu) - E\left(\frac{\pi}{2}, \mu\right)F(\omega, \mu)}{\left[F\left(\frac{\pi}{2}, \mu\right) - F\left(\frac{\pi}{2}, \mu\right)\right]F\left(\frac{\pi}{2}, m\right) + F\left(\frac{\pi}{2}, \mu\right)E\left(\frac{\pi}{2}, m\right)}. \quad (27)$$

The capacitance per unit length corresponding to  $W/D$  from (26) is given by  $C_0^{(2D)} = \epsilon_0 F(\pi/2, \mu) / F(\pi/2, m)$  [94]. Hence, from (25), the average SCLC density is given by

$$J_{2D} = \frac{4}{9} \sqrt{\frac{2e}{m_e}} V_g^{3/2} \frac{\epsilon_0 F\left(\frac{\pi}{2}, \mu\right)}{WDF\left(\frac{\pi}{2}, m\right)}. \quad (28)$$

Taking the ratio of (28) to the 1-D CL law gives the 2-D CL law as

$$\frac{J_{2D}}{J_{1D}} = \frac{F\left(\frac{\pi}{2}, \mu\right) / F\left(\frac{\pi}{2}, m\right)}{W/D}. \quad (29)$$

Since the SCLC density for a 2-D planar diode is independent of  $z$  in Fig. 17, (29) also represents the current density at the cathode [99]. Furthermore, (29) may be used to find the exact SCLC density for a 2-D diode by numerically solving for the complete elliptic integrals.

In addition to the exact solution to (29), we may make two approximations to derive approximate closed form solutions. For  $W/D \gg 1$ , we can use Love's approximation [96], to write (29) to the first order of  $W/D$  as

$$\frac{J_{2D}}{J_{1D}} \approx 1 + \frac{1}{\pi \left(\frac{W}{D}\right)} + \frac{\ln \left(\frac{2\pi W}{D}\right)}{\pi \left(\frac{W}{D}\right)}. \quad (30)$$

From (30),  $J_{2D}/J_{1D} \rightarrow 1$  as  $W/D \rightarrow \infty$ . While the first two terms on the right-hand side of (30) exactly match the 2-D Child-Langmuir solution for emission from a finite emission area along an infinite electrode [100], the third term accounts for the additional contribution of fringing fields for emission from a finite electrode. For  $W/D \ll 1$ , (29) can be approximated as [96]

$$\frac{J_{2D}}{J_{1D}} \approx \frac{\pi}{\left(\frac{W}{D}\right) \ln\left(\frac{4D}{W}\right)} \quad (31)$$

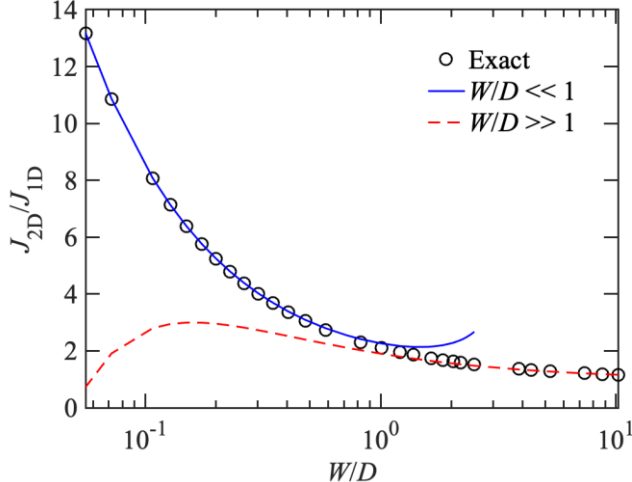


FIG. 18. A semi-log plot of 2-D space-charge limited current  $J_{2D}$  normalized to 1-D space-charge-limited current  $J_{1D}$  as a function of  $\log(W/D)$  for the exact 2-D CL law obtained from (25) and approximations for  $W/D \gg 1$  given by (26) and  $W/D \ll 1$  given by (27) are plotted against  $W/D$ .

Figure 18 compares the exact 2-D CL law and the approximations for large and small values of  $W/D$ . For  $W/D < 0.5$ , (31) is a very good fit to the exact solution from (29); for  $W/D > 2$ , (30) agrees well with (29).

Ongoing work is extending these efforts to 3-D and preparing a manuscript to submit to *Physics of Plasmas*. We are also leveraging this approach to derive analytic equations for SCLC in pin-to-pin, misaligned pin-to-pin, and pin-to-plate geometries and have submitted to *IEEE Transactions on Electron Devices*.

## PIN-TO-PLATE GAS BREAKDOWN

A. M. Loveless<sup>G,P</sup>, L. I. Breen<sup>U</sup>, and A. L. Garner, “Analytic theory for field emission driven microscale gas breakdown for a pin-to-plate geometry,” *Journal of Applied Physics* **129**, 103301 (2021).

Decreasing electronics size necessitates better characterization of electron emission at micro and nanoscales for applications including microplasmas, micro- and nanoelectromechanical systems, and directed energy. While Paschen’s Law (PL) has historically predicted breakdown voltage based on Townsend avalanche, field emission must be incorporated for gap sizes below  $\sim 15 \mu\text{m}$ . Extensive studies have modified PL to explicitly include field emission for planar geometries; however, many practical experiments use pin-to-plate geometries. We modify a previous theory coupling PL and field emission to account for pin-to-plate geometries by replacing the field enhancement, which has been used primarily as a fitting parameter, with the appropriate vacuum

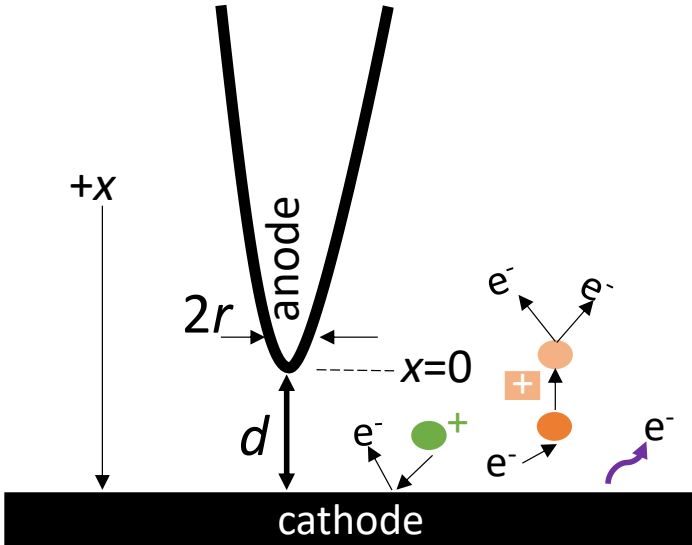


FIG. 19. Pin-to-plate geometry considered in the analysis, where the pin represents the anode set at  $x = 0$  with a tip radius of  $r$  and the plate is the cathode at a gap distance of  $d$  from the tip. Processes for electron emission include secondary electron emission, ionization, and field emission, which creates the space-charge region near the cathode [from Ref. [55]].

ultimately be applied to other nonplanar geometries by applying the appropriate equation for vacuum electric field.

Figure 19 shows the pin-to-plate geometry considered in this analysis with pin anode at  $x = 0$  with a tip radius of  $0.5 \mu\text{m}$ , and a copper plate as the cathode at  $x = d$  set a gap distance of  $1, 5, \text{ or } 10 \mu\text{m} \pm 0.5 \mu\text{m}$  from the tip [69].

Considering the cathode at  $x = d$ , we next incorporate space charge into the total current density through the modified Fowler-Nordheim current as

$$\begin{aligned} \bar{J}'_{tot} &= \frac{\bar{J}'_{FN} \exp\left(\int_0^{\bar{d}} \bar{\alpha}(\bar{x}) d\bar{x}\right)}{\left\{1 - \gamma_{SE} \left[\exp\left(\int_0^{\bar{d}} \bar{\alpha}(\bar{x}) d\bar{x}\right) - 1\right]\right\}} \\ &= \frac{\bar{J}_{FN} (1 + 2 \bar{E}^+(d) / \bar{E}_{tot}(d)) \exp(\bar{E}^+(d) / \bar{E}_{tot}(d))^2 \exp\left(\int_0^{\bar{d}} \bar{\alpha}(\bar{x}) d\bar{x}\right)}{\left\{1 - \gamma_{SE} \left[\exp\left(\int_0^{\bar{d}} \bar{\alpha}(\bar{x}) d\bar{x}\right) - 1\right]\right\}}, \end{aligned} \quad (32)$$

where  $\bar{E}^+(d)$  represents the enhancement in the electric field at the cathode due to the positive space charge induced by the additional ionization due to the electrons that enter the gap due to

electric field. This requires explicitly accounting for the spatial dependence of ionization and non-uniform space charge in Poisson's equation. We derive a breakdown equation of the form previously obtained for planar geometry [101] that agrees well with experimental data with the work function as the fitting parameter. The work function was consistently lower ( $\sim 2 \text{ eV}$ ) than anticipated ( $\sim 4.5 \text{ eV}$ ), but was generally fairly consistent ( $\sim \pm 7 \%$ ). We then derived closed form solutions in the limit of low ionization, corresponding to the field emission regime, and recovered an analytic solution for a parallel plate geometry in the limit of small gap distance that differed from prior analytic results because of the explicit consideration of spatial dependence in charge density. This theory may

field emission. Inserting (32) into the nondimensionalized form of  $j_{tot}$  and assuming  $\bar{\alpha}\bar{d} \ll 1$ , which generally holds until transitioning to PL [54], yields

$$\frac{d\bar{E}_{tot}}{d\bar{x}} \approx \sqrt{\frac{\bar{p}}{\bar{T}}} \frac{\int_0^{\bar{d}} \bar{\alpha}(\bar{x}) d\bar{x} \bar{E}_b^2 \exp(-1/\bar{E}_b) (1 + 2\bar{E}^+(d)/\bar{E}_b) \exp(\bar{E}^+/\bar{E}_b^2)}{\sqrt{\bar{E}_v(\bar{x})} \left(1 - \gamma_{SE} \int_0^{\bar{d}} \bar{\alpha}(\bar{x}) d\bar{x}\right)}, \quad (33)$$

where  $\bar{E}_v(\bar{x}) = \bar{E}_b(\bar{d} + \bar{r})/(2\bar{x} + \bar{r})$  and we have used  $\bar{E}^+(d) \ll \bar{E}_{tot}(d)$  to obtain  $\bar{E}_{tot}(d) \approx \bar{E}_b$  for ultimately determining  $V_b$ . Solving (30) is challenging due to the spatial dependence of  $\bar{E}_v(\bar{x})$ , which comes from the drift velocity  $v_d$ ; however, the variation of  $\bar{E}_v^{1/2}(\bar{x})$  leads to at most a variation in  $v_d$  of  $\sim 20\%$  at  $1\text{ }\mu\text{m}$  and  $< 10\%$  at  $\sim 0.1\text{ }\mu\text{m}$ . Thus, for the purposes of solving (30), we may neglect this spatial variation and set  $\bar{E}_v(\bar{x}) \approx \bar{E}_b$  for simplicity. Given that  $\gamma_{SE} \ll 1$  (generally considered between  $10^{-3}$ - $10^{-1}$  [54] and numerical solutions show that  $\bar{\alpha}\bar{d} \lesssim 15$  prior to transitioning to PL for gaps  $\sim 10\text{ }\mu\text{m}$  [54]. While this assumption may hinder predictive capability in the transition regime between the field emission driven regime and PL,  $\bar{\alpha}\bar{d} \lesssim 0(1)$  at smaller gaps where field emission clearly drives breakdown [54], making this assumption more accurate in the more field emission driven regime. Furthermore, sensitivity analysis using error propagation showed that  $\gamma_{SE}$  had minimal impact on  $V_b$  when field emission dominated in a parallel plate geometry [102], providing additional justification for neglecting this term for calculations in the field emission regime. Thus, we may neglect the second term in the parentheses of the denominator of (30) since  $\gamma_{SE}\bar{\alpha}\bar{d} \ll 1$  in the FE dominant breakdown regime, allowing us to rewrite (33) as

$$\frac{d\bar{E}_{tot}}{d\bar{x}} = -\sqrt{\frac{\bar{p}}{\bar{E}_b \bar{T}}} \bar{E}_b^3 \bar{r} \left[ \exp\left(-\frac{\bar{p}(2\bar{d} + \bar{r})}{\bar{E}_b \bar{r}}\right) - \exp\left(-\frac{\bar{p}}{\bar{E}_b}\right) \right] \exp\left(\frac{-1}{\bar{E}_b}\right) \left(1 + \frac{2\bar{E}^+}{\bar{E}_b}\right) \exp\left(\frac{\bar{E}^+}{\bar{E}_b^2}\right). \quad (34)$$

Integrating (34) across the gap (0 to  $\bar{d}$ ) yields

$$\begin{aligned} \bar{E}_{tot}(\bar{d}) = & \exp\left[\frac{-2\bar{d}\bar{p} - \bar{r} - 2\bar{p}\bar{r}}{\bar{E}_b\bar{r}}\right]\bar{E}_b \left\{ \exp\left[\frac{2\bar{d}\bar{p} + \bar{r} + 2\bar{p}\bar{r}}{\bar{E}_b\bar{r}}\right] \right. \\ & - \bar{d}\bar{E}_b\bar{r} \sqrt{\frac{\bar{p}}{\bar{E}_b\bar{T}}} (\bar{E}_b + 2\bar{E}^+(d)) \exp\left[\frac{\bar{E}^+(d)}{\bar{E}_b^2}\right] \exp\left[\frac{\bar{p}}{\bar{E}_b}\right] \\ & \left. + \bar{d}\bar{E}_b\bar{r} \sqrt{\frac{\bar{p}}{\bar{E}_b\bar{T}}} (\bar{E}_b + 2\bar{E}^+(d)) \exp\left[\frac{\bar{E}^+(d)}{\bar{E}_b^2}\right] \exp\left[\frac{(2\bar{d} + \bar{r})\bar{p}}{\bar{r}\bar{E}_b}\right] \right\}. \end{aligned} \quad (35)$$

This differs from the planar case, which assumed that the space-charge was constant from the center of the gap to the cathode ( $d/2 \leq x \leq d$ ), making  $E^+ \propto d$  [101]. Subtracting  $\bar{E}_b$  from both sides of (35) to obtain  $\bar{E}^+(d)$  on the left-hand-side (LHS) and setting  $y = \bar{E}^+(d)/\bar{E}_b^2$  gives

$$1 = \frac{(1 + 2y\bar{E}_b) \exp[y]}{y} \left\{ \exp\left[\frac{-\bar{r} - \bar{p}\bar{r}}{\bar{E}_b\bar{r}}\right] \bar{d}\bar{r} \sqrt{\frac{\bar{p}}{\bar{E}_b\bar{T}}} \bar{E}_b \right. \\ \left. - \exp\left[\frac{-2\bar{d}\bar{p} - \bar{r} - \bar{p}\bar{r}}{\bar{E}_b\bar{r}}\right] \bar{d}\bar{r} \sqrt{\frac{\bar{p}}{\bar{E}_b\bar{T}}} \bar{E}_b \right\}. \quad (36)$$

Finally, setting the LHS =  $g(y)$  and minimizing (36) yields the breakdown condition as

$$y_0 = \exp\left[\frac{-\bar{r} - \bar{p}\bar{r}}{\bar{E}_b\bar{r}}\right] \bar{d}\bar{r} \sqrt{\frac{\bar{p}}{\bar{E}_b\bar{T}}} \bar{E}_b (1 + 2y_0\bar{E}_b) \exp[y_0] \\ - \exp\left[\frac{-2\bar{d}\bar{p} - \bar{r} - \bar{p}\bar{r}}{\bar{E}_b\bar{r}}\right] \bar{d}\bar{r} \sqrt{\frac{\bar{p}}{\bar{E}_b\bar{T}}} \bar{E}_b (1 + 2y_0\bar{E}_b) \exp[y_0], \quad (37)$$

where  $y_0 = (-1 + \sqrt{1 + 8\bar{E}_b})/(4\bar{E}_b)$ . This is analogous to the final planar breakdown condition [101], but accounts for the nonuniform electric field and resulting non-uniform space charge across the gap for a pin-to-plate geometry.

We first apply the breakdown model described in (37) to experimental data from Ref. [56] using a pin with a 0.5  $\mu\text{m}$  tip radius and gap distances of 1, 5, and 10  $\mu\text{m}$ . Figure 20 shows the fitted  $\phi$  as a function of breakdown event for all data collected in Ref. [56] determined from numerically

solving (37). Because we incorporate the work function into the scaling parameters, changing the work function changes all of the scaling terms for converting from dimensional variables to nondimensional variables, which changes every subsequent variable (all of the dimensionless terms). Thus, care must be taken when comparing nondimensional values for different work functions. We numerically determine  $\phi$  that equates  $\bar{E}_b$  from (37) with the experimentally determined, nondimensionalized breakdown voltage.

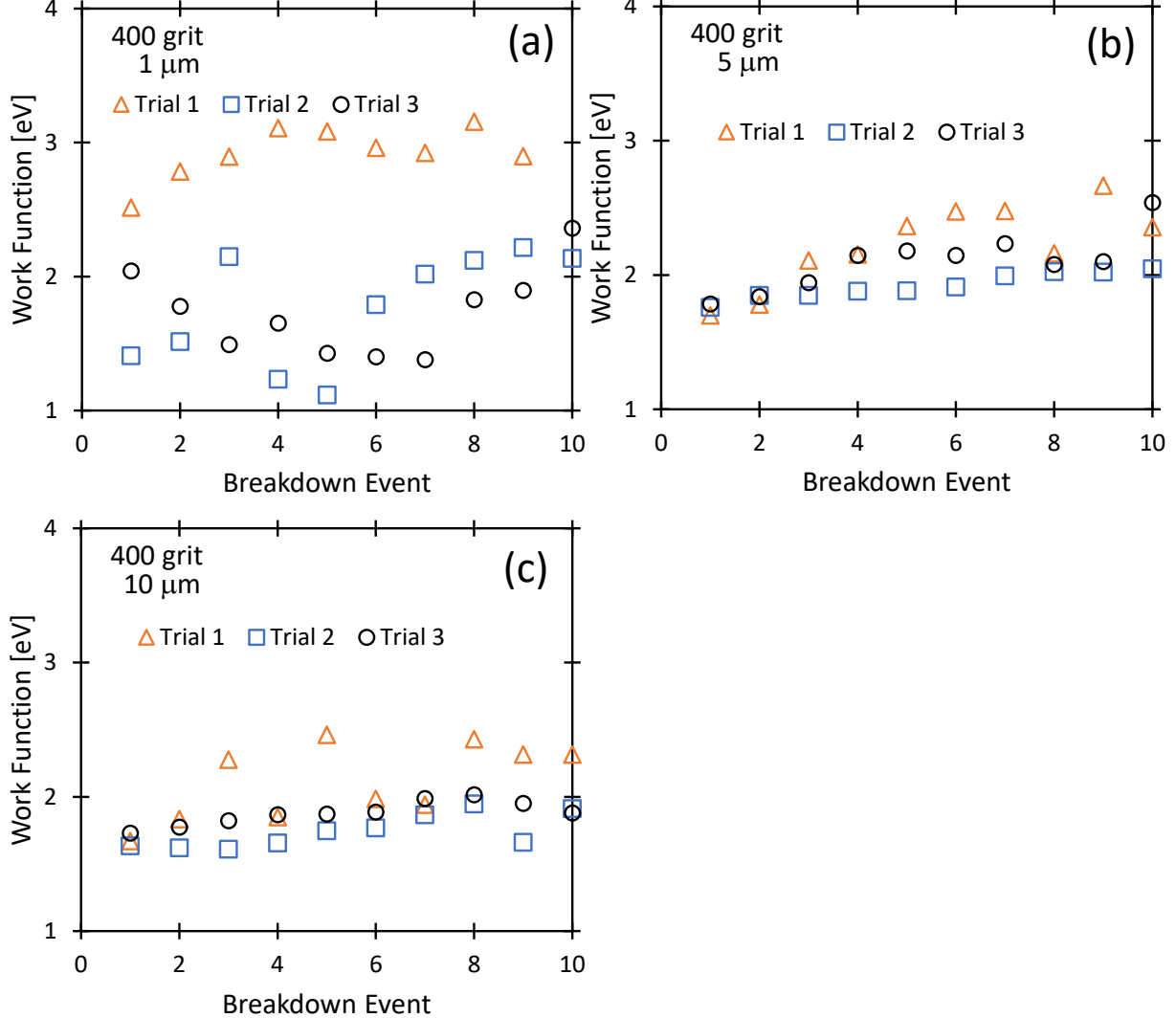


FIG. 20. Work function as a function of breakdown event for 400 grit polishing at initial interelectrode gap distances (neglecting potential changes due to crater formation) of (a) 1  $\mu\text{m}$ , (b) 5  $\mu\text{m}$ , and (c) 10  $\mu\text{m}$ . Each point represents data from each individual breakdown event from Ref. [56] [from Ref. [55]].

## MICROSCALE GAS BREAKDOWN USING A SERIES RESISTOR

Analogous to our previously reported work assessing a series resistor with electron emission, we are currently working with an Undergraduate student participating in our Purdue Summer University Research Fellowship (SURF) to extend the microscale gas breakdown resistance to include the series ballast resistor in our analytic theory and in particle-in-cell simulations. We are currently working on the theory and incorporating the series resistor into XPDP1. Figure 21 shows

preliminary data that shows that the applied voltage is constant with series resistance below a threshold value and begins to increase linearly with resistance above that level. We are currently working to derive asymptotic equations for microscale gas breakdown at low and high resistance to determine a general condition for when resistance becomes important as a function of diode conditions.

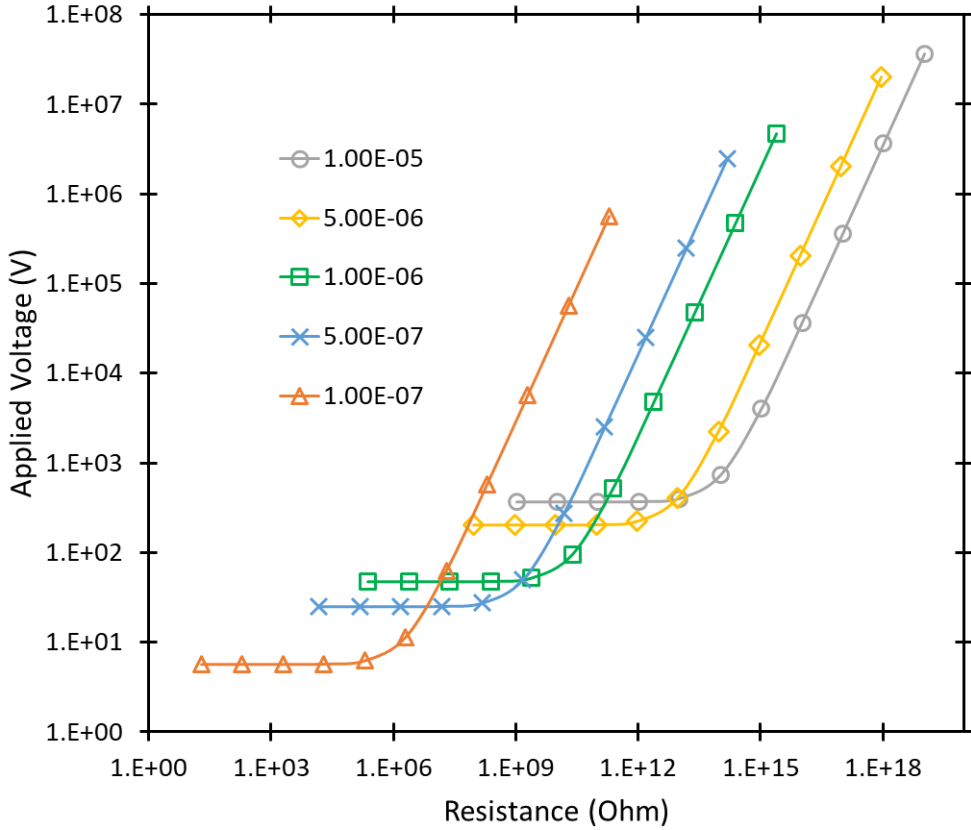


FIG. 21. Theoretical results for applied breakdown voltage as a function of series resistor for five different gap distances. At larger resistance, the applied breakdown voltage increases linearly with increasing resistance.

## STUDENTS SUPPORTED

This grant has partially supported four graduate students during this grant: Adam Darr, Amanda Loveless, Sarah Lang, and N. R. Sree Harsha. Amanda Loveless defended her Ph.D. dissertation in August 2020 and is now a Post-Doctoral Research Associate at Purdue University. Sarah Lang defended her MS thesis in December 2020 and is employed at Los Alamos National Laboratory. Adam Darr completed the Ph.D. candidacy examination in 2019, passed the Ph.D. preliminary examination in 2020, and is scheduled to defend his Ph.D. dissertation in 2022. N. R. Sree Harsha has passed the oral examination for Ph.D. candidacy and will take the remaining oral section in 2022; he is tentatively scheduled to defend his Ph.D. dissertation in 2024. Additionally, Dr. Loveless was a three-time recipient of the Directed Energy Professional Society Scholarship during this period of time (through August 2020) and Adam Darr was a multiple time recipient of the American Nuclear Society Graduate Scholarship.

## REFERENCES

- [1] A. M. Loveless and A. L. Garner, "A universal theory for gas breakdown from microscale to the classical Paschen law," *Phys. Plasmas* **24**, 113522 (2017).
- [2] F. Paschen, "Ueber die zum Funkenuebergang in luft, wasserstoff un Kohlensaeure bei verschiedenen drucken erforderliche potentialdifferenz," *Ann. Phys.* **273**, 69 (1889).
- [3] D. B. Go and A. Venkatraman, "Microscale gas breakdown: ion-enhanced field emission and the modified Paschen's curve," *J. Phys. D.* **47**, 503001 (2014).
- [4] W. S. Boyle and P. Kisliuk, "Departure from Paschen's law of breakdown in gases," *Phys. Rev.* **97**, 255 (1955).
- [5] A. M. Loveless and A. L. Garner, "Scaling laws for gas breakdown for nanoscale to microscale gaps at atmospheric pressure," *Appl. Phys. Lett.* **108**, 234103 (2016).
- [6] G. Meng, X. Gao, A. M. Loveless, G, C. Dong, D. Zhang, K. Wang B. Zhu, Y. Chen, and A. L. Garner, "Demonstration of field emission driven microscale gas breakdown for pulsed voltages using in-situ optical imaging," *Phys. Plasmas* **25**, 082116 (2018).
- [7] R. H. Fowler and L. Nordheim, "Electron emission in intense electric fields," *Proc. R. Soc. London, Ser. A* **119**, 173-181 (1928).
- [8] M. Radmilovic-Radjenovic and B. Radjenovic, "An analytical relation describing the dramatic reduction of the breakdown voltage for the microgap devices," *Eur. Phys. Lett.* **83**, 25001 (2008).
- [9] P. Rumbach and D. B. Go, "Fundamental properties of field emission-driven direct current microdischarges," *J. Appl. Phys.* **112**, 103302 (2012).
- [10] P. Rumbach, Y. Li, S. Martinez, T. J. Twahirwa, and D. B. Go, "Experimental study of electron impact ionization in field emission-driven microdischarges," *Plasma Sour. Sci. Technol.* **23**, 065026 (2014).
- [11] D. B. Go and D. A. Pohlman, "A mathematical model of the modified Paschen's curve for breakdown in microscale gaps," *Phys. Plasmas* **19**, 123515 (2012).
- [12] F. Schertz, M. Schmelzeien, M. Kreiter, H.-J. Elmers, and G. Schönhense, "Field emission of electrons generated by the near field of strongly coupled plasmons," *Phys. Rev. Lett.* **108**, 237602, (2012).
- [13] R. Forbes, "Field emission: new theory for the derivation of emission area from a Fowler-Nordheim plot," *J. Vac. Sci. Technol. B* **17**, 526 (1999).
- [14] R. G. Forbes and J. H. B. Deane, "Reformulation of the standard theory of Fowler-Nordheim tunnelling and cold field electron emission," *Proc. R. Soc. A* **463**, 2907 (2007).
- [15] R. G. Forbes, "Physics of generalized Fowler-Nordheim type equations," *J. Vac. Sci. Technol. B* **26**, 788-793 (2008).
- [16] T. Ito, T. Kanazawa, and Satoshi Hamaguchi, "Rapid breakdown mechanisms of open air nanosecond dielectric barrier discharges," *Phys. Rev. Lett.* **107**, 065002 (2011).
- [17] Y. Y. Lau, Y. Liu, and R. K. Parker, "Electron emission: from the Fowler-Nordheim relation to the Child-Langmuir law," *Phys. Plasmas* **1**, 2082 (1994).
- [18] I. Langmuir, "Electric discharges in gases at low pressures," *J. Franklin Inst.* **214**, 275 (1932).
- [19] P. Zhang, A. Valfells, L. K. Ang, J. W. Luginsland, and Y. Y. Lau, "100 years of the physics of diodes," *Appl. Phys. Rev.* **4**, 011304 (2017).
- [20] K. Jensen, "A tutorial on electron sources," *IEEE Trans. Plasma Sci.* **46**, 1881 (2018).
- [21] C. B. Johnson and H. J. Oskam, "Space-charge-limited current in gas diodes," *J. Appl. Phys.* **42**, 5352 (1971).
- [22] I. Brodie and P. R. Schwoebel, "Vacuum microelectronic devices," *Proc. IEEE* **82**, 1006 (1994).

- [23] I. Langmuir, "Convection and conduction of heat in gases," *Phys. Rev.* **34**, 401 (1912).
- [24] R. Forman, "Electrical conduction and breakdown in high-pressure rare gases," *Phys. Rev. Lett.* **6**, 594 (1961).
- [25] J. R. Smith, J. L. Bilbro, and R. J. Nemanich, "Theory of space charge limited regime of thermionic energy converter with negative electron affinity emitter," *J. Vac. Sci. Technol. B* **27**, 1132 (2009).
- [26] A. H. Khoshaman and A. Nojeh, "A self-consistent approach to the analysis of thermionic devices," *J. Appl. Phys.* **119**, 044902 (2016).
- [27] A. H. Khoshaman and A. Nojeh, "Classical momentum gap for electron transport in vacuum and consequences for space charge in thermionic converters with a grid electrode," *J. Vac. Sci. Technol. B* **34**, 040610 (2016).
- [28] S. Meir, C. Stephanos, T. H. Geballe, and J. Mannhart, "Highly-efficient thermoelectric conversion of solar energy and heat into electric power," *J. Ren. Sustain. Energy* **5**, 043127 (2013).
- [29] A. Agiral and J. G. E. Gardeniers, in: *Proceedings of 2008 IEEE 35th International Conference on Plasma Science*, "Atmospheric Pressure Field Electron Emission from Nanostructures," (IEEE, Karlsruhe, 2008), p. 1.
- [30] S. Brimley, M. S. Miller, and M. J. Hagmann, "Field emission in air and space-charge-limited currents from iridium-iridium oxide tips with gaps below 100 nm," *J. Appl. Phys.* **109**, 094510 (2011).
- [31] J. H. Ingold, "Electron flow in gas diodes. I. transition from inertia-limited flow to mobility-limited flow," *J. Appl. Phys.* **40**, 55 (1969).
- [32] J. H. Ingold, "Electron flow in gas diodes. II. mobility-limited flow for collision frequency proportional to electron speed," *J. Appl. Phys.* **40**, 62 (1969).
- [33] P. V. Akimov and H. Schamel, "Space-charge-limited current in electron diodes under the influence of collisions," *J. Appl. Phys.* **92**, 1690 (2002).
- [34] H. Schamel, "Lagrangian fluid description with simple applications in compressible plasma and gas dynamics," *Phys. Rep.* **392**, 279 (2004).
- [35] R. Forman, "Low-voltage arc and breakdown effects in xenon-filled thermionic diodes," *J. Appl. Phys.* **41**, 4836 (1970).
- [36] R. Forman, "Theory of space-charge-limited emission in high-pressure gas diodes," *J. Appl. Phys.* **34**, 2578 (1963).
- [37] X. Tang and P. K. Shukla, "Child-Langmuir flow in a planar diode filled with charged dust impurities," *Phys. Plasmas* **15**, 023702 (2008).
- [38] L. Oksuz and N. Hershkowitz, "First experimental measurements of the plasma potential throughout the presheath and sheath at a boundary in a weakly collisional plasma," *Phys. Rev. Lett.* **89**, 145001, (2002).
- [39] R. Forman, "Space-charge limited current relation in high-pressure gas diodes," *Phys. Rev.* **123**, 1537 (1961).
- [40] P. V. Akimov, H. Schamel, H. Kolinsky, A. Ya. Ender, and V. I. Kuznetsov, "The true nature of space-charge-limited currents in electron vacuum diodes: A Lagrangian revision with corrections," *Phys. Plasmas* **8**, 3788 (2001).
- [41] X. G. Zhang and S. T. Pantelides, "Theory of space charge limited currents," *Phys. Rev. Lett.* **108**, 266602 (2012).
- [42] N. F. Mott and R. W. Gurney, *Electronic Processes in Ionic Crystals*, (Clarendon Press, Oxford, 1940).

- [43] M. S. Benilov, “The Child-Langmuir Law and analytical theory of collisionless to collision-dominated sheaths,” *Plasma Sources Sci. Technol.* **18**, 014005 (2008).
- [44] J. D. Levine, R. Meyer, R. Baptist, T. E. Felter, and A. A. Talin, “Field emission from microtip test arrays using resistor stabilization,” *J. Vac. Sci. Technol. B* **13**, 474-477 (1995).
- [45] J. W. Luginsland, A. Valfells, and Y. Y. Lau, “Effects of a series resistor on electron emission from a field emitter,” *Appl. Phys. Lett.* **69**, 2770-2772 (1996).
- [46] S. Kunuku, K. J. Sankaran, C-L. Dong, N-H. Tai, K-C. Leou, and I-N. Lin, “Development of long lifetime cathode materials for microplasma application,” *RSC Adv.* **4**, 47865-47875 (2014).
- [47] A. Venkatraman, “Theory and analysis of operating modes in microplasmas assisted by field emitting cathodes,” *Phys. Plasmas* **22**, 057102 (2015).
- [48] A. M. Darr, A. M. Loveless, and A. L. Garner, “Unification of field emission and space charge limited emission with collisions,” *Appl. Phys. Lett.* **114**, 014103 (2019).
- [49] S. D. Dynako, A. M. Darr, and A. L. Garner, “Incorporating resistance into the transition from field emission to space charge limited emission with collisions,” *IEEE J. Electron Dev. Soc.* **7**, 650-654 (2019).
- [50] A. M. Darr, C. R. Darr, and A. L. Garner, “Theoretical assessment of transitions across thermionic, field, and space-charge limited emission,” *Phys. Rev. Res.* **2**, 033137 (2020).
- [51] S. A. Lang, MS Thesis, School of Nuclear Engineering, Purdue University (2020).
- [52] N. R. Sree Harsha and A. L. Garner, “Applying conformal mapping to derive analytical solutions of space-charge-limited current density for various geometries,” *IEEE Trans. Electron Devices* **68**, 264-270 (2021).
- [53] A. M. Darr and A. L. Garner, “A coordinate system invariant formulation for space-charge limited current in vacuum,” *Appl. Phys. Lett.* **115**, 054101 (2019).
- [54] A. L. Garner, A. M. Loveless, J. N. Dahal, and A. Venkatraman, “A tutorial on theoretical and computational techniques for gas breakdown in microscale gaps,” *IEEE Trans. Plasma Sci.* **48**, 808-824 (2020).
- [55] A. M. Loveless, L. I. Breen, and A. L. Garner, “Analytic theory for field emission driven microscale gas breakdown for a pin-to-plate geometry,” *J. Appl. Phys.*, Accepted 13 February 2021.
- [56] R. S. Brayfield, II, A. J. Fairbanks, A. M. Loveless, S. Gao, A. Dhanabal, W. Li, C. Darr, W. Wu, and A. L. Garner, “The impact of cathode surface roughness and multiple breakdown events on microscale gas breakdown at atmospheric pressure,” *J. Appl. Phys.* **125**, 203302 (2019).
- [57] A. L. Garner, G. Meng, Y. Fu, A. M. Loveless, R. S. Brayfield II, and A. M. Darr, “Transitions between electron emission and gas breakdown mechanisms across length and pressure scales,” *J. Appl. Phys.* **128**, 210903 (2020).
- [58] N. M. Zubarev and S. N. Ivanov, “Mechanism of runaway electron generation at gas pressures from a few atmospheres to several tens of atmospheres,” *Plasma Phys. Rep.* **44**, 445–452 (2018).
- [59] G. Meng *et al.*, “Spatio-temporal dynamics of pulsed gas breakdown in micogaps,” *Phys. Plasmas* **26**, 014506 (2019).
- [60] P. Echlin, “Low temperature scanning electron microscopy: a review,” *J. Microsc.* **112**, 47-61 (1978).
- [61] Y. Chen, V. E. Centonze, A. Verkhovsky and G. G. Boris, “Imaging of cytoskeletal elements by low-temperature high resolution scanning electron microscopy,” *J. Microsc.* **179**, 67-76 (1995).
- [62] A. M. Loveless, G. Meng, Q. Ying, F. Wu, K. Wang, Y. Cheng, and A. L. Garner, “The transition to Paschen’s law for microscale gas breakdown at subatmospheric pressure,” *Sci. Rep.* **9**, 5669 (2019).

- [63] K. L. Jensen, J. J. Petillo, E. J. Montgomery, Z. Pan, D. W. Feldman, P. G. O’Shea, N. A. Moody, M. Cahay, J. E. Yater, and J. L. Shaw, “Application of a general electron emission equation to surface nonuniformity and current density variation,” *J. Vac. Sci. Tech. B* **26**, 831 (2008).
- [64] K. L. Jensen, D. W. Feldman, M. Virgo, and P. G. O’Shea, “Measurement and analysis of thermal photoemission from a dispenser cathode,” *Phys. Rev.* **6**, 083501 (2003).
- [65] K. L. Jensen, D. W. Feldman, and P. G. O’Shea, “Time dependent models of field-assisted photoemission,” *J. Vac. Sci. and Tech. B* **23**, 621 (2005).
- [66] K. L. Jensen, D. W. Feldman, N. A. Moody, and P. G. O’Shea, “A photoemission model for low work function coated metal surfaces and its experimental validation,” *J. Appl. Phys.* **99**, 124905 (2006).
- [67] E. Forati and D. Sievenpiper, “Electron emission by long and short lasers: essentials for the design of plasmonic photocathodes,” *J. App. Phys.* **124**, 083101 (2018).
- [68] K. L. Jensen, “General formulation of the thermal, field and photoinduced electron emission,” *J. Appl. Phys.* **102**, 024911 (2007).
- [69] K. L. Jensen, “A quantum dipole-modified work function for a simplified electron emission barrier,” *J. Appl. Phys.* **111**, 054916 (2012).
- [70] K. L. Jensen, “A reformulated general thermal-field emission equation,” *J. Appl. Phys.* **126**, 065302 (2019).
- [71] K. L. Jensen, M. McDonald, O. Chubenko, J. R. Harris, D. Shiffler, N. A., Moody, J. J. Petillo, and A. J. Jensen, “Thermal-field and photoemission from meso- and micro-scale features: Effects of screening and roughness on characterization and simulation,” *J. Appl. Phys.* **125**, 234303 (2019).
- [72] J. K. Bragg, A. H. Sharbaugh, and R. W. Crowe, “cathode effects in dielectric breakdown of liquids,” *J. Appl. Phys.* **25**, 382 (1954).
- [73] B. Halpern and R. Gomer, “Field emission in liquids,” *J. Chem. Phys.* **43**, 1069 (1965).
- [74] B. Halpern and R. Gomer, “Field emission in liquids,” *J. Chem. Phys.* **51**, 1031 (1969).
- [75] B. Halpern and R. Gomer, “Field ionization in liquids,” *J. Chem. Phys.* **51**, 1048 (1969).
- [76] A. H. Sharbaugh, J. C. Devins, and S. J. Rzad, “Progress in the field of electric breakdown in dielectric liquids,” *IEEE Trans. Electr. Insul.* **EI-13**, 249 (1978).
- [77] W. F. Schmidt, “Electronic conduction processes in dielectric liquids,” *IEEE Trans. Electr. Insul.* **EI-19**, 389 (1984).
- [78] P. V. E. McClintock, “Field emission in liquid helium,” *Phys. Lett.* **29A**, 453-454 (1969).
- [79] J. Qian, R. P. Joshi, J. Kolb, K. H. Schoenbach, J. Dickens, A. Neuber, M. Butcher, M. Cevallos, H. Krompholz, E. Schamiloglu, J. Gaudet, “Microbubble-based model analysis of liquid breakdown initiation by a submicrosecond pulse,” *J. Appl. Phys.* **97**, 113304 (2005).
- [80] N. Phan, B. Beaumont, N. Bouman, S. Clayton, S. Currie, T. Ito, J. Ramsey, G. Seidel, and W. Wei, “Understanding electrical breakdown in liquid helium with a statistical distribution-based study,” in Fall Meeting of the APS Divison of Nuclear Physics Virtual (2020).
- [81] M. Auger, A. Blatter, A. Ereditato, D. Göldi, S. Jano, I. Kreslo, M. Lüthi, C. R. von Rohr, T. Strauss, M. S. Weber, “On the electric breakdown in liquid argon at centimeter scale,” *J. Instrum.*, **11**, P03017 (2016).
- [82] A. L. Garner, A. Caiafa, Y. Jiang, S. Klopman, C. Morton, A. S. Torres, A. M. Loveless, and V. B. Neculaes, “Experimental validation of a compact, flexible pulsed power architecture for ex vivo platelet activation,” *PLoS ONE* **12**, e0181214 (2017).

- [83] L. Xu, A. L. Garner, B. Tao, and K. M. Keener, "Microbial inactivation and quality changes in orange juice treated by high voltage atmospheric cold plasma," *Food Bioprocess Technol.* **10**, 1778-1791 (2017).
- [84] J.E. Foster, "Plasma-based water purification: Challenges and prospects for the future," *Phys. Plasmas* **24**, 055501 (2017).
- [85] C. P Bankston, L. H. Back, E. Y. Kwack, and A. J. Kelly, "Experimental investigation of electrostatic dispersion and combustion of diesel fuel jets," *J. Eng. Gas Turb. Power* **110**, 361-368 (1988).
- [86] D. Krejci, F. Mier-Hicks, R. Thomas, T. Haag, and P. Lozano, "Emission characteristics of passively fed electrospray microthrusters with propellant reservoirs," *J. Spacecraft Rockets* **54**, 447-458 (2017).
- [87] S. Marcuccio, A. Genovese, and M. Andrenucci, "Experimental performance of field emission microthrusters," *J. Propul. Power* **14**, 774-781 (1998).
- [88] I. Levchenko, S. Xu, S. Mazouffre, D. Lev, D. Pedrini, D. Goebel, L. Garrigues, F. Taccogna, and K. Bazaka, "Perspectives, frontiers, and new horizons for plasma-based space electric propulsion," *Phys. Plasmas* **27**, 020601 (2020).
- [89] S. Bhattacharjee and T. Chowdhury, "Experimental investigation of transition from Fowler-Nordheim field emission to space-charge-limited flows in a nanogap," *Appl. Phys. Lett.* **95**, 061501 (2009).
- [90] K. Dotoku, H. Yamada, S. Sakamoto, S. Noda, and H. Yoshida, "Field emission into nonpolar organic liquids," *J. Chem. Phys.* **69**, 1121 (1978).
- [91] S. A. Lang, A. M. Darr, and A. L. Garner, "Theoretical analysis of the transition from field emission to space-charge-limited emission in liquids and gases," *J. Appl. Phys.* **128**, 185104 (2020).
- [92] A. M. Loveless, A. M. Darr, and A. L. Garner, "Linkage of electron emission and breakdown mechanism theories from quantum scales to Paschen's law," *Phys. Plasmas* **28**, 042110 (2021).
- [93] U. Tiwary and B. N. Basu, "Noniterative method for the synthesis of convergent Pierce electron guns," *IEEE Trans. Electron Devices* **35**, 1218-1222 (1988).
- [94] H. F. Ivey, "Approximate solutions of the space-charge problem for some unusual electrode geometries," *J. Appl. Phys.* **24**, 1466-1472 (1953).
- [95] J. D. Jackson, *Classical Electrodynamics*, Singapore: Wiley and Sons Pte. Ltd., (1999), p. 53.
- [96] H. B. Palmer, "The capacitance of a parallel-plate capacitor by the Schwartz-Christoffel transformation," *Trans. AIEEE.*, **56**, 363-366 (1937).
- [97] H. Hancock, *Elliptic Integrals*, 1<sup>st</sup> ed., New York: John Wiley and Sons, Inc., (1917), p. 15.
- [98] V. V. Batygin and I. N. Toptygin, *Problems in Electrodynamics*, 2<sup>nd</sup> ed. London: Academic Press Inc. (1978), p. 249-250.
- [99] A. Rokhlenko and J. L. Lebowitz, "Space-charge-limited 2D electron flow between two flat electrodes in a strong magnetic field," *Phys. Rev. Lett.* **91**, 085002 (2003).
- [100] Y. Y. Lau, "Simple theory for the two-dimensional Child-Langmuir law," *Phys. Rev. Lett.* **87**, 278301 (2001).
- [101] A. Venkattraman and A. A. Alexeenko, "Scaling law for direct current field emission-driven microscale gas breakdown," *Phys. Plasmas* **19**, 123515 (2012).
- [102] S. Dynako, A. M. Loveless, and A. L. Garner, "Sensitivity of modeled microscale gas breakdown voltage due to parametric variation," *Phys. Plasmas* **25**, 103505 (2018).

## ARCHIVAL OUTPUT

**Published Refereed Journal Articles** (underline = student or postdoctoral research associate author, <sup>G</sup> = Graduate Student, <sup>U</sup> = Undergraduate Student):

10. A. M. Loveless<sup>G</sup>, A. M. Darr<sup>G</sup>, and **A. L. Garner**, “Linkage of Electron Emission and Breakdown Mechanism Theories from Quantum Scales to Paschen’s Law,” *Physics of Plasmas* **28**, 042110 (2021).
9. [INVITED PERSPECTIVE, FEATURED ARTICLE] P. Zhang, Y. S. Ang, **A. L. Garner**, Á. Valfells, J. W. Luginsland, and L. K. Ang, “Space-charge limited current in nanodiodes: Ballistic, Collisional and Dynamical Effects,” *Journal of Applied Physics* **129**, 100902 (2021).
8. A. M. Loveless<sup>G,P</sup>, L. I. Breen<sup>U</sup>, and **A. L. Garner**, “Analytic theory for field emission driven microscale gas breakdown for a pin-to-plate geometry,” *Journal of Applied Physics* **129**, 103301 (2021).
7. N. R. Sree Harsha<sup>G</sup> and **A. L. Garner**, “Applying Conformal Mapping to Derive Analytical Solutions of Space-Charge-Limited Current Density for Various Geometries,” *IEEE Transactions on Electron Devices* **68**, 264-270 (2021).
6. [INVITED PERSPECTIVE] **A. L. Garner**, G. Meng, Y. Fu, A. M. Loveless<sup>G,P</sup>, R. S. Brayfield II<sup>G</sup>, and A. M. Darr<sup>G</sup>, “Transitions between electron emission and gas breakdown mechanisms across length and pressure scales,” *Journal of Applied Physics* **128**, 210903 (2020).
5. S. A. Lang<sup>G</sup>, A. M. Darr<sup>G</sup>, and **A. L. Garner**, “Theoretical analysis of the transition from field emission to space-charge-limited emission in liquids and gases,” *Journal of Applied Physics* **128**, 185104 (2020).
4. A. M. Darr<sup>G</sup>, C. R. Darr<sup>U</sup>, and **A. L. Garner**, “Theoretical Assessment of Transitions across Thermionic, Field, and Space-Charge Limited Emission,” *Physical Review Research* **2**, 033137 (2020).
3. [INVITED MINI-COURSE] **A. L. Garner**, A. M. Loveless<sup>G</sup>, J. N. Dahal, and A. Venkatraman, “A Tutorial on Theoretical and Computational Techniques for Gas Breakdown in Microscale Gaps,” *IEEE Transactions on Plasma Science* **48**, 808-824 (2020).
2. S. D. Dynako<sup>U</sup>, A. M. Darr<sup>G</sup>, and **A. L. Garner**, “Incorporating Resistance into the Transition from Field Emission to Space Charge Limited Emission with Collisions,” *IEEE Journal of the Electron Devices Society* **7**, 650-654 (2019).
1. A. M. Darr<sup>G</sup>, A. M. Loveless<sup>G</sup>, and **A. L. Garner**, “Unification of field emission and space charge limited emission with collisions,” *Applied Physics Letters* **114**, 014103 (2019).

**Submitted or to be Submitted Refereed Journal Article** (underline = student or postdoctoral research associate author, <sup>G</sup> = Graduate Student, <sup>U</sup> = Undergraduate Student):

5. N. R. Sree Harsha<sup>G</sup> and **A. L. Garner**, “Analytic Solutions for Space-Charge-Limited Current Density from a Sharp Tip,” Submitted.
4. N. R. Sree Harsha<sup>G</sup> and **A. L. Garner**, “Applying variational calculus and vacuum capacitance to derive the multi-dimensional Child-Langmuir law,” To Be Submitted.

3. S. A. Lang<sup>G</sup>, A. M. Darr<sup>G</sup>, and **A. L. Garner**, “Unification of photoemission with field, space-charge limited, and thermionic emission,” To Be Submitted.
2. J. C. Welch<sup>U</sup>, A. M. Darr<sup>G</sup>, A. M. Loveless<sup>P</sup>, and **A. L. Garner**, “Modification of Field Emission Driven Microscale Gas Breakdown by a Series Resistor,” To Be Submitted.
1. J. M. Halpern<sup>U</sup>, A. M. Darr<sup>G</sup>, N. R. Sree Harsha<sup>G</sup>, and **A. L. Garner**, “Application of Variational Calculus and Conformal Mapping to Space-charge Limited Current with Nonzero Injection Velocity,” To Be Submitted.

**Conference Poster Presentation** [presenter in *italics*]:

7. J. Halpern<sup>U</sup>, A. Darr<sup>G</sup>, and **A. Garner**, “Coordinate System Invariant Space Charge Limited Current for General Initial Velocity,” 62nd Annual Meeting of the American Physical Society Division of Plasma Physics, JP13.00098, 10 November 2020.
6. N. R. Sree Harsha<sup>G</sup> and **A. L. Garner**, “Analytical Solution for Space Charge Limited Current Emission from a Sharp Tip Using Variational Methods,” IEEE International Vacuum Electronics Conference, P8.22, 22 October 2020.
5. C. Darr<sup>U</sup>, A. Darr<sup>G</sup>, S. Lang<sup>G</sup>, and **A. Garner**, “Transitions between Thermionic, Field, and Vacuum Space Charge Limited Emission,” American Physical Society Division of Plasma Physics, Bull. Am. Phys. Soc., Vol. 64, NP10.00009 (2019).
4. A. M. Loveless<sup>G</sup>, A. M. Darr<sup>G</sup>, R. S. Brayfield II<sup>G</sup>, J. R. Malayter<sup>U</sup>, S. A. Lang<sup>G</sup>, and **A. L. Garner**, “The Implications of Nanoscale Features for Microscale and Smaller Gaps on Electron Emission,” Joint Meeting of the 32<sup>nd</sup> International Vacuum Nanoelectronics Conference (IVNC) and 12<sup>th</sup> International Vacuum Electron Sources Conference (IVESC), Cincinnati, OH, 18.1, 24 July 2019.
3. S. Lang<sup>U</sup>, **A. Garner**, and A. Darr<sup>G</sup>, “Unification of Thermionic, Field, and Space Charge Limited Emission,” IEEE Pulsed Power and Plasma Science Conference, 1P10, 24 June 2019, Orlando, FL USA.
2. S. Lang<sup>U</sup> and **A. Garner**, “Electron emission in liquids,” IEEE Pulsed Power and Plasma Science Conference, IEEE Pulsed Power and Plasma Science Conference, 1P09, 24 June 2019, Orlando, FL, USA.
1. **A. L. Garner**, A. M. Darr<sup>G</sup>, and A. M. Loveless<sup>G</sup>, “Incorporating Collisions into the Transition from Field Emission to Space Charge Limited Flow,” 2018 IEEE International Conference on Plasma Sciences, P2A-1346-1, 27 June 2018, Denver, CO USA.

**Conference Plenary Talk** [Presenter in *italics*]

1. **A. L. Garner**, “Diode Physics: From Child-Langmuir to Paschen’s Law,” 2021 IEEE International Conference on Plasma Sciences, to be presented in September 2021.

### **Conference Invited Talks [Presenter in *italics*]**

3. A. M. Loveless<sup>P</sup>, A. M. Darr<sup>G</sup>, and A. L. Garner, “Electron Emission Nexus Theory for a Crossed-Field Diode,” 2021 IEEE International Conference on Plasma Sciences, to be presented in September 2021.

2. A. L. Garner, A. M. Loveless<sup>G</sup>, R. S. Brayfield II<sup>G</sup>, A. M. Darr<sup>G</sup>, J. R. Malayter<sup>U</sup>, and G. Meng, “Gas Breakdown and Electron Emission for Microscale Gaps: Unified Theory and Nanofeature Effects,” Joint Meeting of the 32<sup>nd</sup> International Vacuum Nanoelectronics Conference (IVNC) and 12<sup>th</sup> International Vacuum Electron Sources Conference (IVESC), Cincinnati, OH, 13.1, 25 July 2019.

1. A. L. Garner, A. M. Loveless<sup>G</sup>, R. S. Brayfield II<sup>G</sup>, A. J. Fairbanks<sup>G</sup>, S. D. Dynako<sup>U</sup>, S. Gao<sup>G</sup>, W. Wu, R. S. Bean, and G. Meng, “Gas Breakdown at Microscale and Smaller Gaps: Theoretical Unification of Mechanisms and Experimental Assessment of Surface Roughness,” iPlasmaNanoIX, New Buffalo, MI, 27 August 2018.

### **Conference Oral Presentations [Presenter in *italics*]**

23. N. R. Sree Harsha<sup>G</sup> and A. L. Garner, “Multi-dimensional space-charge limited current using variational calculus and vacuum capacitance,” IEEE International Conference on Plasma Science, to be presented.

22. S. A. Lang<sup>G</sup>, A. M. Darr<sup>G</sup>, and A. L. Garner, “Unification of photo-, thermionic, and field emission,” IEEE International Conference on Plasma Science, to be presented.

21. H. Wang<sup>G</sup>, R. S. Brayfield II, A. Venkatraman, A. M. Loveless<sup>P</sup>, C. J. Buerke<sup>U</sup>, and A. L. Garner, “Calculation of ionization coefficient in microscale and nanoscale gaps using PIC/MCC simulations,” IEEE International Conference on Plasma Science, to be presented.

20. J. M. Halpern<sup>U</sup>, A. M. Darr<sup>G</sup>, N. R. Sree Harsha<sup>G</sup>, and A. L. Garner, “Space-charge-limited current for nonzero electron injection velocity in non-planar diodes,” IEEE International Conference on Plasma Science, to be presented.

19. J. C. Welch III<sup>U</sup>, A. M. Darr<sup>G</sup>, and A. L. Garner, “Determination of applied voltage from gas breakdown for microscale to classical Paschen law with a resistor,” IEEE International Conference on Plasma Science, to be presented.

18. S. A. Lang<sup>G</sup>, A. M. Darr<sup>G</sup>, and A. L. Garner, “Theoretical Examination of electron emission liquids to gases,” IEEE International Conference on Plasma Science, TA1-S1-060, Session D1N1-TA1:1, 06 December 2020.

17. A. M. Darr<sup>G</sup>, A. M. Loveless<sup>P</sup>, R. S. Brayfield<sup>G</sup>, H. Wang<sup>G</sup>, and A. L. Garner, “Nexus Theory: electron emission regime transitions across length, pressure, and temperature scales,” IEEE International Conference on Plasma Science, TA3-S1-066, Session D1N3-TA3.1, 06 December 2020.

16. A. Loveless<sup>G,P</sup>, L. Breen<sup>U</sup>, R. Brayfield<sup>G</sup>, and A. Garner, “A Universal Theory for Microscale Gas Breakdown for a Pin to Plate Geometry,” 62<sup>nd</sup> Annual Meeting of the American Physical Society Division of Plasma Physics, NO03.00010, 11 November 2020.

15. S. Lang<sup>G</sup>, A. Darr<sup>G</sup>, and **A. Garner**, “Theoretical analysis of the transition from field emission to space-charge limited emission in liquids,” 62<sup>nd</sup> Annual Meeting of the American Physical Society Division of Plasma Physics, NO03.00009, 11 November 2020.
14. Sree Harsha N R<sup>G</sup> and **A. L. Garner**, “Conformal Mapping for Calculating Space Charge Limited Current,” 62<sup>nd</sup> Annual Meeting of the American Physical Society Division of Plasma Physics, BO03.00013, 09 November 2020.
13. A. M. Loveless<sup>P</sup>, A. M. Darr<sup>G</sup>, and **A. L. Garner**, “Transitions in Electron Emission and Gas Breakdown from Nanoscale to Microscale,” IEEE Vacuum Electronics Conference, 20 October 2020.
12. A. M. Darr<sup>G</sup>, C. R. Darr<sup>U</sup>, and **A. L. Garner**, “Nexus between Field, Thermionic, and Space-Charge Limited-Emission Theories,” IEEE Vacuum Electronics Conference, 20 October 2020.
11. R. S. Brayfield II<sup>G</sup>, A. M. Darr<sup>G</sup>, W. Li<sup>U</sup>, A. J. Fairbanks<sup>G</sup>, H. Wang<sup>G</sup>, A. M. Loveless<sup>G</sup>, and **A. L. Garner**, “Nano/Micro-Meter electrode topology Effects on Electron Emission,” 22nd Annual Directed Energy Science & Technology Symposium, Student Workshop, 11 March 2020, West Point, NY, USA.
10. A. M. Loveless<sup>G</sup>, A. M. Darr<sup>G</sup>, and **A. L. Garner**, “Implications of Electrode Geometry on Electron Emission and Microscale Gas Breakdown,” 22nd Annual Directed Energy Science & Technology Symposium, Student Workshop, 11 March 2020, West Point, NY, USA.
9. A. M. Loveless<sup>G</sup>, A. M. Darr<sup>G</sup>, R. S. Brayfield II<sup>G</sup>, J. R. Malayter<sup>U</sup>, S. A. Lang<sup>G</sup>, and **A. L. Garner**, “Nanoscale Feature Implications on Electron Emission and Gas Breakdown,” Trans. Am. Nucl. Soc. **121**, 399-401 (2019).
8. A. Darr<sup>G</sup>, A. Loveless<sup>G</sup>, and **A. Garner**, “Incorporating Resistance into the Unification of Field Emission and Space Charge-Limited Emission with Collisions,” IEEE Pulsed Power and Plasma Science Conference, 7A3, 27 June 2019.
7. A. Loveless<sup>G</sup>, A. Darr<sup>G</sup>, and **A. Garner**, “Electron Emission and Gas Breakdown: Unification of Theory from Schrodinger’s Equation to Paschen’s Law,” IEEE Pulsed Power and Plasma Science Conference, 3F2, 25 June 2019.
6. A. M. Loveless<sup>G</sup>, A. M. Darr<sup>G</sup>, S Dynako<sup>U</sup>, and **A. L. Garner**, “Transition of Electron Emission and Gas Breakdown Mechanisms from Microscale to Nanoscale,” 21st Annual Directed Energy Science & Technology Symposium, Student Workshop I, 09 April 2019, Destin, FL, USA.
5. A. Loveless<sup>G</sup>, A. Darr<sup>G</sup>, S. Dynako<sup>U</sup>, and **A. Garner**, “Unification of Gas Breakdown and Electron Emission,” American Physical Society March Meeting 2019, Bull. Am. Phys. Soc., Vol. 64, R18.00004 (2019).
4. S. Dynako<sup>U</sup>, A. Darr<sup>G</sup>, and **A. Garner**, “Incorporating collisions and resistance into the transition from field emission to the space charge regime regime,” American Physical Society Division of Plasma Physics, Vol. 63, NO8.00006 (2018).
3. A. Loveless<sup>G</sup> and **A. Garner**, “Electron Emission and Gas Breakdown from Schrödinger’s Equation to Paschen’s Law,” American Physical Society Division of Plasma Physics, Vol. 63, NO8.00002 (2018).

2. S. D. Dynako<sup>U</sup>, A. M. Darr<sup>G</sup>, and **A. L. Garner**, "Incorporating collisions and resistance into the transition from field emission to the space charge regime," The Summer Undergraduate Research Fellowship (SURF) Symposium, 02 August 2018, West Lafayette, IN USA, p.89.
1. A. M. Loveless<sup>G</sup>, A. M. Darr<sup>G</sup>, S. D. Dyanko<sup>U</sup>, and **A. L. Garner**, "Transition from Microscale to Nanoscale Breakdown Dynamics," 2018 IEEE International Conference on Plasma Sciences, O3A-2, 26 June 2018, Denver, CO USA.

### **Invited Seminars**

13. **A. L. Garner**, "Modified Paschen's law for Microscale and Nanoscale Gaps," Michigan Institute of Plasma Science and Engineering, Ann Arbor, MI, 13 October 2020. (Delivered remotely due to COVID-19).
12. **A. L. Garner**, "Re-envisioning Electron Emission Physics," Sandia National Laboratories, Albuquerque, NM, 17 August 2020. (Delivered remotely due to COVID-19).
11. **A. L. Garner**, "Unified Electron Emission Theory and Experimental Validation," Oak Ridge National Laboratory, Oak Ridge, TN, 03 March 2020.
10. **A. L. Garner**, "Unified Electron Emission Theory and Experimental Validation," Department of Electrical and Computer Engineering, University of New Mexico, Albuquerque, NM, 06 December 2019.
9. **A. L. Garner**, "Theoretical and Experimental Unification of Electron Emission Mechanisms," Department of Electrical and Computer Engineering, Boise State University, Boise, ID, 04 December 2019.
8. **A. L. Garner**, "Electron Emission and Gas Breakdown from Quantum to Classical Lengths," Plasma Seminar Series, University of Washington, Seattle, WA, 02 December 2019.
7. **A. L. Garner**, "Progress Toward a Universal, Unified Electron Emission Theory," Air Force Research Laboratory, Air Force Research Laboratory, Albuquerque, NM, 11 July 2019.
6. **A. L. Garner**, "Unification of Electron Emission and Gas Breakdown Mechanisms: Experiment and Theory," Sandia National Laboratories, Albuquerque, NM, 10 July 2019.
5. **A. L. Garner**, "Unification of Breakdown Theories across Gap and Pressure," Army Research Laboratory, Aberdeen, MD, 12 July 2018.
4. **A. L. Garner**, "The Influence of Gap Size and Electrode Surface on Gas Breakdown and Electron Emission," Naval Surface Warfare Center Dahlgren Division, Dahlgren, VA, 11 July 2018.
3. **A. M. Loveless**<sup>G</sup>, "Unification of gas breakdown laws across frequency and gap distance," Naval Research Laboratory, 10 July 2018.
2. **A. L. Garner**, "The Influence of Gap Size and Electrode Surface on Gas Breakdown and Electron Emission," Varex Imaging, Salt Lake City, UT, 07 June 2018.

1. **A. L. Garner**, “Gas Breakdown and Electron Emission for Microscale and Smaller Gaps,” Naval Surface Warfare Center Crane, Crane, IN, 03 May 2018.

**Mini-courses and Special Presentations**

1. **A. L. Garner**, “Microscale to Nanoscale Gas Breakdown: From Paschen’s Law to Schrödinger’s Equation,” Mini-course on Theoretical and Computational Methods in Plasma Physics, 2019 Pulsed Power and Plasma Science Conference, Orlando, FL, 23 June 2019.